Phosphorylated tau in the retina correlates with tau pathology in the brain in Alzheimer's disease and primary tauopathies

Frederique J. Hart de Ruyter[1,2], Tjado H.J. Morrema[1], Jurre den Haan[2], Netherlands Brain Bank[3], Jos W.R. Twisk[4], Johannes F. de Boer[5], Philip Scheltens[2], Baayla D.C. Boon[1,2,6], Dietmar R. Thal[7], Annemieke J. Rozemuller[1], Frank D. Verbraak[8], Femke H. Bouwman[2,9], Jeroen J.M. Hoozemans[1,9]

1 Amsterdam UMC location Vrije Universiteit Amsterdam, Pathology, Amsterdam, De Boelelaan 1117, Amsterdam, The Netherlands
2 Alzheimer Center Amsterdam, Neurology, Vrije Universiteit Amsterdam, Amsterdam UMC location VUmc, Amsterdam, The Netherlands
3 Netherlands Institute for Neuroscience, Meibergdreef 47, 1105 BA, Amsterdam, the Netherlands
4 Amsterdam UMC location Vrije Universiteit Amsterdam, Epidemiology and Data Science, Amsterdam, De Boelelaan 1117, Amsterdam, The Netherlands
5 Vrije Universiteit Amsterdam, LaserLaB, Physics and Astronomy, Amsterdam, The Netherlands
6 Mayo Clinic, Neuroscience, Jacksonville, Florida, USA
7 KU Leuven, Leuven Brain Institute, 3000 Leuven, Belgium; Laboratory for Neuropathology, Department of Imaging and Pathology, KU Leuven, and Department of Pathology, UZ Leuven, 3000 Leuven, Belgium
8 Amsterdam UMC location Vrije Universiteit Amsterdam, Ophthalmology, Amsterdam, De Boelelaan 1117, Amsterdam, The Netherlands
9 Amsterdam Neuroscience, Neurodegeneration, Amsterdam, the Netherlands

Frederique J. Hart de Ruyter and Tjado H.J. Morrema are co-first authors.

Corresponding author:
Jeroen J.M. Hoozemans, jjm.hoozemans@amsterdamumc.nl, +31204444444
Frederique J. Hart de Ruyter, f.hartderuijter@amsterdamumc.nl, +31204440912

Acknowledgements
We would like to acknowledge all donors and their caregivers. We thank N.P. Smoor for his technical expertise and assistance in retinal tissue preparation. We thank Michiel Kooreman for helping with clinical data retrieval and his assistance at the Netherlands Brain Bank in collecting brain sections. We thank Jacoline B. ten Brink and Arthur A.B. Bergen for their technological support and advice on the retina. We thank Gina Gase for technical assistance with tissue preparation and immunohistochemistry. We thank A. Dijkstra for contributing to the assessment of the visual system. Illustration was created with BioRender.com.

Author contributions

All authors contributed to the study conception and design. Experiments were performed by T.H.J. Morrema. Data collection and analysis were performed by F.J. Hart de Ruyter and T.H.J. Morrema. The first draft of the manuscript was written by F.J. Hart de Ruyter and J.J.M. Hoozemans. All authors commented on previous versions of the manuscript. All authors read and approved the final manuscript.

Compliance with Ethical Standards

Ethical approval: Donors signed informed consent for brain and eye autopsy and use of brain and retinal tissue and medical records for research prior to death. This study was approved by the ethical committee of the VU University Medical Center Amsterdam (VUmc).

Funding

This research was funded by the Netherlands Organisation for Scientific Research (NWO, MEDPHOT P18-26 Project 5).

Abstract

The retina is a potential source of biomarkers for the detection of neurodegenerative disease. Accumulation of phosphorylated tau (p-tau) in the brain is a pathological feature characteristic for Alzheimer's disease (AD) and primary tauopathies. In this study the presence of p-tau in the retina in relation to tau pathology in the brain was assessed. Post-mortem eyes and brains were collected through the Netherlands Brain Bank from donors with AD (n=17), primary tauopathies (n=8), α-synucleinopathies (n=13), other neurodegenerative diseases including non-tau frontotemporal lobar degeneration (FTLD) (n=9), and controls (n=15). Retina cross-sections were assessed by immunohistochemistry using antibodies directed against total tau (HT7), 3R and 4R tau isoforms (RD3, RD4), and phospho-epitopes Ser202/Thr205 (AT8), Thr217 (anti-T217), Thr212/Ser214 (AT100), Thr181 (AT270), Ser396 (anti-pS396) and Ser422 (anti-pS422). Retinal tau load was compared to p-tau Ser202/Thr205 and p-tau Thr217 load in various brain regions. Total tau, 3R and 4R tau isoforms were most prominently present in the inner plexiform layer (IPL) and outer plexiform layer (OPL) of the retina and were detected in all cases and controls as a diffuse and somatodendritic signal. Total tau, p-tau Ser202/Thr205 and p-tau Thr217 was observed in amacrine and horizontal cells of the inner nuclear layer (INL). Various antibodies directed against phospho-epitopes of tau showed immunoreactivity in the IPL, OPL, and INL. P-tau Ser202/Thr205 and Thr217 showed significant discrimination between AD and other tauopathies, and non-tauopathy cases including controls. Whilst immunopositivity was observed for p-tau Thr212/Ser214, Thr181 and Ser396, there were no group differences. P-tau Ser422 did not show any immunoreactivity in the retina. The presence of retinal p-tau Ser202/Thr205 and Thr217 correlated with Braak stage for NFTs and with the presence of p-tau Ser202/Thr205 in hippocampus and cortical brain regions. Depending on the phospho-epitope, p-tau in the retina is a potential biomarker for AD and primary tauopathies.

Keywords: Retina, eye, tau, phosphorylation, post-mortem, Alzheimer's disease, tauopathies, neurodegeneration.

Introduction

There is a growing interest in the eye, and in particular the retina, as a potential source of biomarkers for Alzheimer's disease (AD) and other neurodegenerative diseases. The neuropathological hallmarks of AD – the most common cause of dementia – include neuronal loss, extra-cellular amyloid-beta (Aβ) plaques and neurofibrillary tangles (NFTs)[4]. NFTs are primarily composed of intracellular aggregates of hyper-phosphorylated micro-tubule associated tau protein. The hyper-phosphorylation of tau inhibits its function in microtubule assemblage, promotes its aggregation into oligomers and fibrils, and eventually forms filamentous aggregates called NFTs[5]. The phosphorylation and aggregation of tau is a major constituent of AD and primary tauopathies like frontotemporal lobar degeneration (FTLD)-tau[16], progressive supranuclear palsy (PSP) and corticobasal degeneration (CBD)[48]. Phosphorylated tau (p-tau) also accumulates in primarily age-related neurodegeneration such as primary age-related tauopathy (PART)[10] and aging-related tau astrogliopathy (ARTAG)[29].

The retina – embryologically derived from the diencephalon – is an extension of the central nervous system and shows many similarities with the brain in terms of anatomy and functionality[32]. The axons of retinal ganglion cells form the optic nerve providing a direct connection to the central nervous system. Retinal neuronal cells have functional properties similar to central neuronal cells[32]. The eye contains a blood-retina barrier similar to the blood-brain barrier, and the aqueous humor in the anterior eye segment shares similarities with cerebrospinal fluid in the brain [26, 32, 42, 45]. In addition, the retina and the brain undergo similar age-related and hereditary degeneration, which may be caused by altered expression of neuron-related proteins[31]. Because of these common features and the direct connection to the brain, changes present in the retina could be indicative of changes in the brain. This supports the potential of examining the eye with noninvasive imaging techniques aiming to diagnose neurodegenerative diseases[32].

Similar to the brain, tau is highly expressed in the retina. The presence of tau is primarily observed in the inner plexiform layer (IPL), outer plexiform layer (OPL), and inner nuclear layer (INL) of the retina[31]. Accumulation of non-phosphorylated tau has been observed in photoreceptor cells and retinal ganglion cells[30]. Schön and colleagues[40] were the first to demonstrate disease-associated p-tau in AD post-mortem retinas, which was confirmed by other studies[12, 18]. In these studies, the presence of p-tau was observed as a diffuse staining in the IPL and OPL, as well as in retinal ganglion cells. Overall p-tau is increased in AD retina yet does not show presence of fibrillar tau aggregates or NFTs[12, 18, 40]. It is important to note that cohorts were small (up to 10 AD cases per study) and there are also reports that could not observe abnormalities related to tau pathology in the retina[20, 21, 46].

Although previous post-mortem studies described the presence of p-tau in AD retina[12, 40], some questions remain unanswered. At this moment it is not clear if the presence of p-tau is specific for AD or if p-tau is also present in the retina of other (primary) tauopathies or other neurodegenerative diseases. In addition, no data is available on the correlation between tau pathology in the retina and the brain, and if its presence follows the hierarchical distribution of NFT tau pathology as proposed by Braak and Braak[4]. Another question that remains unanswered is whether the retina shows a similar presence of tau phospho-epitopes compared with the brain. Elucidating the above would extend our understanding in the underlying disease mechanism in the retina and the potential of p-tau in the retina

as biomarker. The aim of this study was to assess the presence of different phospho-epitopes of tau in post-mortem retina tissue in relation to tau pathology in the brain in a cohort of AD cases, primary tauopathies and other non-tau neurodegenerative diseases compared to controls with or without accumulation of p-tau in the brain.

Materials and methods

Post-mortem tissue

Post-mortem brain tissue and eyes of 62 donors were obtained by the Netherlands brain bank (NBB, Amsterdam, The Netherlands, https://www.brainbank.nl). All donors gave informed consent for the use of their brain and eyes as well as clinical records for research purposes in compliance with ethical standards. The VUmc medical ethics committee approved the donor program of the NBB. Extensive clinical history was available and brain autopsies were performed according to the Code of Conduct of Brain Net Europe[27]. Subjects were included based on availability from 2009 until 2020 and had a variety of neuropathological diagnoses.

Brain tissue was collected within 12 hours post-mortem and subsequently formalin-fixed (10%; 4 weeks) and paraffin-embedded (FFPE). Neuropathological assessment was performed by an experienced neuropathologist (AR), according to the NIA-AA criteria including Braak stage for NFTs[4] and Lewy bodies[1], Thal phase for Aβ [23, 43], and CERAD score for neuritic plaque pathology[35]. Based on neuropathological diagnosis, cases were categorized into the following groups: AD[23] (n=17), primary tauopathies[13, 15, 29] (n=8), α-synucleinopathies[25, 33] (n=13), other neurodegenerative diseases (n=9) and controls (n=15). Controls had no clinical cognitive complaints, and were stratified based on the Braak stage for NFTs in two groups; controls without p-tau in the brain (Braak stage 0; n=6), and controls with p-tau in the brain (Braak stage I ≥ III; n=9). Cohort characteristics are shown in Table 1. A medical history record of ophthalmologic disease was not an exclusion-criterium for this study. Four cases had posterior segment pathology including retinal detachment (#7, #32), age-related macular degeneration (#14) and optic neuritis (#49).

Post-mortem retinal tissue preparation

Post-mortem interval of retinal tissue is described separately in Table 1. Post-mortem enucleation of eyes was sometimes performed after brain autopsy, therefore indicating a longer post-mortem interval. Eye tissue processing was performed by removing the anterior part of the eye, containing cornea and lens, and filling the eyecup with tissue-tek O.C.T. compound (Sakura, Tokyo, Japan). Either the eye was frozen using iso-pentane at -90 °C and stored at -80 °C, or the eye was directly collected in 4% paraformaldehyde (PFA) and stored for 48 hours before further processing. Frozen eyes were defrosted at room temperature (RT) in PFA for 48 hours prior to dissection. The eye was dissected through the horizontal and vertical axis, resulting in temporal-superior, temporal-inferior, nasal-superior and nasal-inferior quadrants as previously described[12]. Prior to embedding, the quadrants were dehydrated using the following protocol: 3 hours in 4% PFA at 35 °C, 1 hour in 70% ethanol at 35 °C, 1 hour in 80% ethanol at 35°C, 1 hour in 96% ethanol at 35 °C, 3 times for 1 hour in 100% alcohol at 35 °C, 3 times for 1 hour in xylene at 35 °C, and four times for 1 hour in paraffin at 62 °C.

Immunohistochemistry

Tissue sections from FFPE retina at 10 μm thickness of the superior quadrant were sequentially mounted on TOMO glass slides (Matsunami, Osaka, Japan). Brain tissue at 5 μm thickness were mounted on Superfrost plus glass slides (VWR, Pennsylvania, USA). For this study the following brain

regions were separately assessed; the middle hippocampus at the geniculate body, lateral geniculate nucleus (LGN), superior colliculus, temporal pole, medial frontal gyrus, inferior parietal lobe and occipital pole V1/V2. Slides were air dried overnight at 37 °C prior to staining. Sections were deparaffinized and rehydrated using sequential incubations in xylene, alcohol and water. Endogenous peroxidase activity was suppressed by incubating the slides with 0.3% H_2O_2 in phosphate buffered saline pH 7.4 (PBS) (30 min). Antigen retrieval was performed in 10 mM/L citrate buffer (pH 6.0) and heated using an autoclave (20 min. at 121°C). Sections were incubated with primary antibodies against total tau (HT7), 3R tau, 4R tau, p-tau Ser202/Thr205 (AT8), p-tau Thr217 (anti-T217), p-tau Thr212/Ser214 (AT100), p-tau Thr181 (AT270), p-tau Ser396 (anti-pS396) and p-tau Ser422 (anti-pS422) (Table 2, Fig. 1) diluted in antibody diluent (Sigma-Aldrich, Saint Louis, USA) overnight at RT. Of each sequential section series of approximately 20 sections per donor, the first and last section was stained for p-tau in order to confirm p-tau status. Immunohistochemistry was performed on all quadrants in AD cases negative for p-tau Ser202/Thr205 or Thr217. Omission of primary antibody was used as a negative control. After primary antibody incubation the slides were washed in PBS and incubated with anti-mouse/rabbit HRP Envision (DAKO, Glostrup, Denmark) (30 min) and subsequently washed using PBS. 3,3'-Diaminobenzine (DAB; DAKO) was used as a chromogen for color development (5 min) at RT. Sections were counterstained with hematoxylin, dehydrated using alcohol and xylene and mounted using Quick-D (Klinipath; Duiven, The Netherlands).

Fluorescent double-immunostainings

Colocalization of total tau (HT7), p-tau Ser202/Thr205 and p-tau Thr217 with retinal neuronal cells was visualized in a subset of cases using antibodies against calbindin D28K and calretinin. Omission of primary antibody and staining of single antibodies were used as technical controls. Endogenous autofluorescence was negligible and therefore quenching of autofluorescence was not applied. Deparaffinization, citrate antigen retrieval using an autoclave and blocking of endogenous peroxidase activity were performed as described above. For fluorescent double-immunostainings with p-tau Ser202/Thr205, sections were incubated overnight at RT using with a mix of anti-calbindin D28K + p-tau Ser202/Thr205 or anti-calretinin + p-tau Ser202/Thr205 diluted in antibody diluent (Sigma). As secondary step for the mouse antibody (AT8), anti-mouse HRP Envision (DAKO, 30 min. incubation) was used followed by incubation with fluorescein labeled tyramide (AKOYA, Marlborough MA, USA) (10 min). For the rabbit primary antibodies (anti-calbindin D28K or anti-calretinin), goat anti-rabbit IgG Alexa Fluor Plus 594 (ThermoFisher, Waltham MA, USA) was used as a secondary step in a 1:250 dilution in antibody diluent for 1 hour. In between incubations, sections were washed with PBS at RT. To obtain fluorescent double-immunostainings with total tau and p-tau Thr217 (rabbit/rabbit stainings), sections were incubated with HT7 or anti-T217 antibodies diluted in antibody diluent (Sigma) and incubated overnight at RT. As secondary step for the tau antibodies, anti-mouse/rabbit HRP Envision (DAKO, 30 min. incubation) was used followed by incubation with fluorescein labeled tyramide (AKOYA, 10 min. incubation). Primary and secondary antibodies were removed by cooking the sections using a microwave for 10 minutes. Subsequently, the sections were incubated with either calbindin D28K or calretinin diluted in antibody diluent overnight at RT. For the rabbit primary antibodies (anti-calbindin

D28K or anti-calretinin), goat anti-rabbit IgG Alexa Fluor Plus 594 (ThermoFisher) was used as a secondary step in a 1:250 dilution in antibody diluent for 1 hour. In between incubations, sections were washed with PBS at RT. After completion of the stainings sections were coverslipped with DAPI Fluoromount-G (SouthernBiotech, Birmingham AL, USA).

Images were obtained using a Leica DMi8 inverted fluorescence microscope equipped with a Leica DFC300 G camera and illuminated by a mercury light source using LAS AF software (version 1.5). Single plane images using a HCX-PL-fluotar 40x/0.75 lens were made with DAPI (excitation: 325-375; emission: 435-485), FITC (excitation: 460-500; emission: 512-542) and Texas-red (excitation: 540-580; emission: 592-668) filter cubes. Exposure of images was set to a near black image in the negative control slide (Supplementary fig. 1, online resource) at a resolution of 4 pixels per μm. Images of the far peripheral region from three representative cases were made and analyzed using ImageJ software (National Institute of Health). All figures were composed with Adobe Photoshop (Adobe Systems Incorporated, RRID:SCR_014199), version 23.5.

Assessment and quantification of tau immunoreactivity

DAB stained whole-sections were imaged using an Olympus VS200 slide-scanner. Cross-sections of the retina were assessed at three regions of interest (ROI) with an average size of 26000 μm^2; the far peripheral region, mid peripheral region and central region. For selection of the ROIs, points of orientation were used as follows; 1) the beginning of the far peripheral region was marked based on the visibility of the INL and outer nuclear layer (ONL) closest to the ora serrata, 2) the mid peripheral region was identified by thickening of the ONL, 3) the central region was identified closest to the optic nerve, without inclusion of the macula. Sections were quantified by assessing the percentage DAB positive surface area (mean surface %) at the best fit threshold using QuPath (RRID:SCR_018257) version 0.2.0 m12[2] (Supplementary fig. 2, online resource). For detection of positive staining, the down-sample factor was set at 1, Gaussian sigma at 0.25 μm and the haematoxylin threshold ('Negative') at 1 optical density (OD) units. DAB threshold was set at 0.1 OD units for total tau, 0.2 OD units for p-tau Ser202/Thr205, 0.15 OD units for p-tau Thr217, 0.3 OD units for p-tau Ser212/Thr214, 0.8 OD units for p-tau Thr181 and 0.25 OD units for p-tau Ser396. In brain tissue, p-tau Ser202/Thr205 and Thr217 immunoreactivity was assessed using a semi-quantitative score with an Olympus BX41 microscope in the grey matter of the whole brain section with total surface areas ranging from 2 to 4 cm^2. Positive staining was scored as none, few, moderate and high (Supplementary fig. 3, online resource). Assessment of tau pathology in the brain and the retina was performed separately and blinded for diagnosis.

Statistical analysis

Statistical analysis to study group differences was performed using a one-way ANOVA with post hoc analysis (Bonferroni) for continuous data and Chi square testing for dichotomous data. Statistical analysis for group differences of p-tau in the retina, the relation between retinal p-tau Ser202/Thr205 and Thr217 mean surface % and p-tau Ser202/Thr205 and Thr217 in the brain tissue, and the between-region differences for total tau and the different phospho-epitopes (p-tau Ser202/Thr205, Thr217,

Thr212/Ser214, Thr181 and Ser396) was performed using linear mixed models since it accounts for repeated regional measures within the same case being related as opposed to regional measures in other cases. Spearman's correlation was performed to analyze the correlation between p-tau in the retina and Braak stage. Statistical analyses were corrected for age at death and gender and was performed using SPSS Statistics (IBM SPSS Statistics, RRID:SCR_016479) version 26. A *P*-value of <0.05 was considered significant.

Results

Cohort description

Individual case details are reported in Table 1 and group demographics are described in Table 3. To study the clinical relevance of tau in the retina, groups were categorized by neuropathological diagnosis. Age at death was different between groups ($F(5, 56) = 6.92$, $P < 0.001$)). There was a significant difference in post-mortem interval between controls with Braak stage I-III and α-synucleinopathies ($F(5, 56) = 3.38$, $P < 0.05$)). No group difference was found for gender (X^2 (1, 62) = 0.07, $P = 0.80$)). Defined as such, AD cases had significantly higher Braak stages for NFTs, Thal amyloid phase and CERAD score for neuritic plaques.

Localization of phosphorylated tau and tau isoforms in the retina

Characterization of the antibodies used in this study has been assessed previously [6, 11, 17, 24, 34, 37, 39, 44]. To illustrate immunoreactivity of these antibodies in the brain, immunohistochemistry was performed on the medial frontal gyrus of representative cases for each group (Fig. 2). Total tau and p-tau was observed in all AD and tauopathy cases. Tau isoform 3R was observed in AD and tauopathies, except PSP and CBD cases, and 4R tau was seen in all AD and tauopathy cases in this cohort. P-tau epitopes showed variably intense immunoreactivity in control Braak stage II-III revealing few neuropil threads, AD revealing many neuropil threads, NFTs and neuritic plaques and PSP revealing tufted astrocytes. No p-tau immunoreactivity was observed in the medial frontal cortex of control Braak stage 0, FTLD-TDP or PD. The presence and localization of total tau, tau isoforms and p-tau were assessed in cross-sections of the superior retina (Fig. 3) where, as reported previously, AD-associated pathology seems consistently and most prominently present[12, 28]. In all cases and controls, total tau assessed with antibody HT7 was primarily present in the IPL and OPL (Fig. 3, Fig. 4a). This staining pattern was also observed with antibodies specific for the 3R and 4R isoforms of tau. A similar layer distribution was observed for tau phosphorylated at Ser202/Thr205, Thr217, Thr212/Ser214, Thr181 and Ser396. Presence and intensity of immunoreactivity was variable between cases. Immunoreactivity for p-tau Ser202/Thr205 and Thr217 showed a difference in presence and intensity between cases and controls, while Thr212/Ser214, Thr181 and Ser396 showed intense immunoreactivity in all controls and neurodegenerative cases. Immunoreactivity for p-tau Thr181 was also observed in the photoreceptor inner segment (Fig. 4b). A similar distribution was sporadically observed with p-tau Ser396 (Fig. 3). While AD brain tissue showed a clear presence of p-tau Ser422 (Fig. 2), no immunoreactivity for this epitope was observed in the retina in any of the control- or neurodegenerative cases.

In general, immunostaining for total tau with HT7 and p-tau antibodies revealed a diffuse staining of the OPL (Fig. 4a) and distinctive sublaminar layers in the IPL (Fig. 4b). In addition, p-tau and total tau also revealed intracellular signal in the INL and OPL (Fig. 4d). As reported previously, there were no structures observed resembling fibrillar inclusions, threads or neurofibrillary tangles[12]. A more prominent localization of p-tau Ser202/Thr205 was observed in the far periphery as opposed to the mid periphery ($\beta = -11.76$, SE = 1.28, $p < 0.001$) and the central retina ($\beta = -21.92$, SE = 1.44, $p < 0.001$) (Fig. 4e). This gradient was also observed for total tau and all other p-tau epitopes (Supplementary fig. 4, online resource). Some cases showed signal for p-tau Ser202/Thr205 and Thr217 in only one of the

plexiform layers. For example, two CBD (#33, #34), one PSP (#36), one control (#10) and one AD case (#25) showed immunostaining only in the IPL and scarcely in the OPL (Fig. 4f). Other cases primarily showed immunostaining in the OPL, namely one PSP (#35), two AD (#23, #32), and one FTLD-TDP case (#43). In these cases, total tau immunostaining (HT7) was observed in both IPL and OPL.

Total tau, p-tau Ser202/Thr205 and p-tau Thr217 were assessed with calretinin and calbindin D28K to study their presence in neuronal cells (Fig. 5). While calretinin is a marker specific for amacrine cells, and calbindin D28K is a marker for horizontal cells[19], the latter is also present in bipolar cells and cones[38]. Consistent with the literature, calbindin D28K was indeed observed in what are likely to be horizontal cells and cones, while calretinin was detected in presumably amacrine cells and their processes. Co-localization with total tau, p-tau Ser202/Thr205 and Thr217 was observed in horizontal cells and amacrine cells in the INL and the processes of amacrine cells in the IPL.

P-tau in the retina is increased in AD, primary tauopathies and controls with increased presence of cerebral p-tau

Given the significant predilection of p-tau for the far and mid peripheral region of the retina, its presence was quantified separately in these regions only (Table 5). P-tau Ser202/Thr205 and Thr217 was increased in the far periphery in controls with Braak stage I-III, AD cases and primary tauopathies compared with Braak stage 0 control cases (Fig. 6). Primary tauopathies showed increased levels of p-tau Thr217 and Thr181 in both the far and mid periphery, p-tau Ser202/Thr205 in the far periphery and Thr212/Ser214 in the mid periphery. Total tau was relatively high in all groups, including controls. A significant increase in total tau was detected in the far periphery in primary tauopathies compared with Braak stage 0 control cases. P-tau Ser396 immunoreactivity was also relatively high in all groups but did not show any group differences. Overall, p-tau Ser202/Thr205 and Thr217 were increased in groups associated with cerebral tau-pathology, and almost absent in the non-tau associated neurodegenerative disease groups (α-synucleinopathies and other neurodegenerative diseases) and controls without cerebral tau (Braak stage 0).

On a group level, p-tau Ser202/Thr205 and Thr217 immunoreactivity was increased in AD and primary tauopathies. However, 6 out of 17 AD cases (#17, #18, #19, #29, #30, #31) and one FTLD-tau case (#37, Braak stage II) did not show immunoreactivity for p-tau Ser202/Thr205 or Thr217 in the retina. Of these cases, additional sections of all other quadrants were assessed and found negative for p-tau Ser202/Thr205 and Thr217. Of the 6 AD cases without p-tau Ser202/Thr205 or Thr217 immunoreactivity in the retina, half had an atypical neuropathological presentation of AD showing predominantly parietal pathology load in the cerebral cortex (#17, #30, #31)[3].

P-tau Ser202/Thr205 in the retina correlates with tau pathology in the brain

Although significant group differences for p-tau Ser202/Thr205 and Thr217 immunoreactivity in the retina were observed, the variety in controls and AD cases was substantial. Therefore, the relation between p-tau in the retina and tau pathology in the cerebral cortex was further explored. Retinal p-tau Ser202/Thr205 and Thr217 correlated with the Braak stage for NFTs, both showing a positive correlation (p-tau Ser202/Thr205, $rs[59] = 0.35$, $p < 0.01$; p-tau Thr217, $rs[58] = 0.41$, $p < 0.01$). Retinal

immunoreactivity for p-tau Ser202/Thr205 and Thr217 was compared with a semi-quantitative score for p-tau Ser202/Thr205 or Thr217 load in different brain regions (Fig. 7). Immunoreactivity for p-tau Ser202/Thr205 in the far periphery of the retina correlated with p-tau Ser202/Thr205 immunoreactivity in the hippocampus (β = 4.69, SE = 2.05, p = 0.02), temporal pole (β = 6.25, SE = 1.85, p < 0.01), medial frontal gyrus (β = 5.93, SE = 2.06, p < 0.01) and the parietal lobe (β = 5.57, SE = 2.04, p < 0.01). No correlation was found with the occipital pole (β = 2.95, SE = 2.07, p = 0.15). No correlation was observed between retinal Thr217 and p-tau Thr217 immunoreactivity scores in the brain. P-tau Thr217 in the retina correlated with p-tau Ser202/Thr205 in the hippocampus (β = 3.28, SE = 1.22, p < 0.01) and temporal lobe (β = 2.60, SE = 1.11, p = 0.02), however not in the other assessed brain regions (medial frontal gyrus; β = 2.07, SE = 1.24, p = 0.10; parietal lobe; β = 1.48, SE = 1.24, p = 0.23; occipital pole; β = 2.03, SE = 1.43, p = 0.16).

To rule out an effect of ophthalmologic pathology on tau load in the retina, all analyses were additionally performed after exclusion of the cases with posterior segment pathology (#7, #14, #32, #49). The exclusion of these cases did not change the statistical outcome, i.e. significant differences observed between groups and the correlations with brain tau load remained the same.

Patterns of p-tau Ser202/Thr205 immunoreactivity in the visual system

To investigate if p-tau in the retina is part of a hierarchical distribution of tau pathology in the brain, different structures of the visual system were assessed in a subset (N=14) for which brain tissue was available of the LGN and/or superior colliculus (Table 4, Fig. 8). Immunohistochemistry for p-tau Ser202/Thr205 revealed few thread-like structures and neuronal cytoplasmic inclusions in the LGN of all assessed AD and tauopathy cases and was absent in control cases. Of the 8 AD cases in this group, 2 cases (#29, #30) had no p-tau Ser202/Thr205 immunoreactivity in the retina. One control case (#11, Braak stage II) showed high levels of p-tau Ser202/Thr205 immunoreactivity in the retina and mild p-tau Ser202/Thr205 positivity in the occipital pole without the presence of NFTs. The two FTLD-tau cases showed variable p-tau Ser202/Thr205 signal in the visual system; one without p-tau Ser202/Thr205 immunoreactivity in the retina and with p-tau Ser202/Thr205 load in all three regions (#37), and one with high levels for p-tau Ser202/Thr205 immunoreactivity in the retina without p-tau Ser202/Thr205 load in the occipital pole (#38). Although the retina of one FTLD-tau case (#37) did not show p-tau Ser202/Thr205 in the retina, the superior colliculus showed coiled bodies, diffuse positive neurons and high glial and neuronal tau load. Within the superior colliculus, moderate (AD, n=5) to many (primary tauopathies, n=3) p-tau Ser202/Thr205 positive threads, and more sporadically neuritic plaques and dystrophic neurites were observed. The distribution of p-tau Ser202/Thr205 in the visual system of these selected cases was variable and no clear hierarchical distribution could be observed.

Discussion

In this study, increased levels of tau phosphorylated at epitopes Ser202/Thr205 and Thr217 in the retina were observed in AD cases, primary tauopathies and controls with tau pathology in the brain, as opposed to other neurodegenerative cases and controls without tau pathology in the brain. There is a positive correlation between retinal p-tau Ser202/Thr205 and Thr217 with Braak stage for NFTs, and a statistically significant relation between retinal p-tau Ser202/Thr205 and Thr217 immunoreactivity and the presence of p-tau Ser202/Thr205 in hippocampus and cortical brain regions. Results from this study suggest that pathological tau load in the retina mirrors tau pathology in the brain. While the retina is a potential source of biomarkers for the detection of neurodegenerative pathology in the brain, it is important to understand the relation between retina and the brain in the pathogenesis of neurodegenerative diseases. In this study, the presence of p-tau in the retina was assessed in a well-characterized autopsy confirmed cohort with different neurodegenerative diseases and cognitively normal controls with and without cortico-cerebral tau pathology.

The observation of p-tau in AD retinas is in concordance with previous studies[12, 40]. We observed that p-tau and tau isoforms mainly show a diffuse signal in the IPL and OPL, and a somatodendritic immunostaining in the INL. The distinct tau-positive layers observed within the IPL most likely represent anatomical sublaminar layers of the IPL made out of the axons and dendrites from retinal ganglion cells, amacrine cells and bipolar cells[14]. P-tau immunoreactivity in the OPL most likely derives from horizontal cells located in the INL[19]. Interestingly, the presence of p-tau in the IPL and OPL varied between cases. For example, a difference in p-tau immunoreactivity between the IPL and OPL was observed for p-tau Ser202/Thr205 and Thr217 in CBD and PSP, suggesting variable tau phosphorylation by amacrine and horizontal cells[9]. We found that tau and p-tau was mainly present in the far periphery of the retina as previously shown by other groups[12, 22]. This finding could be explained by regional differences in gene expression, structure (i.e. layer thickness and cell type proportion) and metabolism regarding environmental specific stress response and neurotrophic survival factors[47].

Intracellular p-tau immunoreactivity was observed in what are assumed to be horizontal and amacrine cells, using calbindin D28K and calretinin as neuronal markers, respectively. Although intracellular p-tau staining was detected, these structures did not resemble NFTs, one of the hallmarks of AD pathology in the brain. The absence of NFTs in the retina is in concordance with previous studies [12, 40] and supported by the absence of immunoreactivity for p-tau Ser422, which in the brain strongly associates with late-stage AD pathology and NFTs[7]. The absence of retinal structures resembling NFTs or neuropil threads, and the predilection in synaptic layers, indicates that disease-associated retinal p-tau is morphologically different in the retina compared to the brain, and that retina and brain have different response mechanisms associated with tau pathology. The overall high levels of other p-tau epitopes such as p-tau Thr212/Ser214, Thr181 and Ser396 indicate a physiological role for tau phosphorylation in the retina. Group differences found for p-tau Ser202/Thr205 and Thr217 in this study could indicate a disturbance in this physiological process. Whether the presence of p-tau in the retina resembles an early stage of tau pathology that does not progress, or is a completely different metabolic mechanism remains elusive and needs to be addressed in future studies.

A consistent finding of the current study is that controls without tau pathology in the brain do not show p-tau Ser202/Thr205 or Thr217 signal in the retina. P-tau Ser202/Thr205 and Thr217 was present in 5 out of 15 controls, however these cases had a Braak stage of I or II. Similarly, p-tau Ser202/Thr205 and Thr217 signal in the retina was also seen in two neurodegenerative diseases not primarily associated with tau (FTLD-TDP, #43; PDD, #57) however with extensive AD co-pathology in the brain. This implies that the presence of p-tau in the retina may mirror p-tau load in the brain in non-symptomatic individuals with AD pathology, which is supported by studies using AD mouse models showing that p-tau is present in the retina preceding brain pathology[8, 28, 40]. Interestingly, in this study 35% of AD cases had no retinal p-tau Ser202/Thr205 or Thr217 signal. This is in line with findings from earlier studies[12, 18, 21] among which Schön and colleagues[40], who attributed the loss of p-tau Ser202/Thr205 signal to the high post-mortem interval of 72 hours. However, the post-mortem interval of the p-tau Ser202/Thr205 negative cases in this study was not different from that of p-tau Ser202/Thr205 positive cases (7-11 hours), indicating that there might be a different explanation for this finding. Interestingly, three AD cases with no p-tau Ser202/Thr205 or Thr217 immunoreactivity in the retina presented with an atypical spreading of tau pathology in the brain, suggesting that the retina might be differently involved depending on the distribution of tau pathology in the brain[36]. It should be noted that the subset of AD cases with atypical neuropathology in this study is very small (n = 4), and more cases will have to be studied to further elucidate a possible relation with atypical AD. To evaluate the involvement of the retina in the spreading of tau-pathology through the brain along hierarchical pathways [4], the presence of p-tau was assessed in the visual system encompassing LGN, superior colliculus, and occipital pole in a subset of cases. All cases with a Braak stage > 0 showed presence of p-tau Ser202/Thr205 in the LGN and superior colliculus, suggesting that the optic tract is involved in the pathological spreading of p-tau. However, no clear relation between the presence of p-tau Ser202/Thr205 in the retina and p-tau Ser202/Thr205 in the visual system was observed. This argues against involvement of the retina as part of a hierarchical spreading pattern of tau pathology in brain.

Some limitations apply to the current study. Although currently this is the largest post-mortem cohort analyzed with respect to the combination of retina and brain tissue, the tissue for the assessment of the visual system was retrieved retrospectively, and therefore the number of cases was limited. Furthermore, in this study we observed no visual differences for total tau and 3R and 4R tau isoforms. Interestingly, total tau levels assessed with HT7 showed a significant increase in the far periphery of the retina in primary tauopathies. Quantitative assessment of 3R and 4R tau isoforms would be of interest when larger group samples for 3R and 4R tauopathies are available. A technical limitation is the difference in fixation times for retina and brain tissue (48 hours for retina tissue versus 4 weeks for brain tissue). This could explain a difference in the detection of p-tau in retina as compared to brain. In addition, the presence of tau in the retina in this study was assessed in cross-sections, allowing assessment of the different layers of the retina. Future studies will need to address the spatial localization of p-tau in flat-mount preparations, as well as potential differences between the left and right eye. The correlation between retinal p-tau Ser202/Thr205 and age at death indicates an age-effect for p-tau in the retina. Nonetheless, group differences remained significant after correcting for age at death as a confounder. Additionally, there was no difference in age at death between controls with Braak stage

0 and primary tauopathies – including PART and ARTAG – groups between which significant differences in p-tau levels were observed. The effect of age on the presence of p-tau in the retina needs to be elucidated in future studies with larger cohorts.

This study contributes to further development of biomarkers in the eye for neurodegenerative diseases. Our results show that differences in p-tau are predominantly observed in the far periphery of the retina. This implicates that in-vivo scanning studies should consider measuring the far peripheral retina using novel ophthalmologic devices with widefield imaging technology. Structural changes observed with optical coherence tomography [41] could be related to the presence of retinal tau, which in this study was shown to be variable in AD cases. This stresses the need to obtain pre-mortem in-vivo imaging data in combination with post-mortem assessment of structural and biochemical changes in the retina. In addition, future studies should focus on expanding the variety of neurodegenerative diseases, particularly primary tauopathies, such as PSP, CBD and FTLD-tau (Pick's disease, Parkinsonism linked to FTLD-17). Studying more AD cases with atypical neuropathological distribution may shed light on a possible association between atypical tau pathology in the brain and the presence or absence of p-tau in the retina. Currently, there is no fluorophore available for in-vivo ophthalmic detection of (non-fibrillar) p-tau. Development of these fluorophores would require extensive neuropathological investigation before they can be used in clinical practice.

Conclusion

Depending on the epitope, the retina shows increased p-tau in AD and primary tauopathies at group level. Elevated levels of p-tau at epitopes Ser202/Thr205 and Thr217 in the retina correspond with tau pathology in the brain. Cognitively normal controls without cerebral p-tau do not show retinal p-tau at epitopes Ser202/Thr205 and Thr217. This study indicates that when there is p-tau in the retina, there is p-tau in the brain. These results support the development of in-vivo retinal imaging techniques for neurodegenerative diseases. The retina could be a source of biomarkers that helps identify people with presymptomatic stages of neurodegenerative diseases associated with brain tau pathology.

Availability of data and materials

Most data generated or analyzed during this study are included in this published manuscript and the supplementary material. Additional data are available from the corresponding author on reasonable request.

Declarations

Competing interests

F.J. Hart de Ruyter reports no competing interests; T.H.J. Morrema reports no competing interests; Dr. J. den Haan reports no competing interests; Prof. dr. J.W.R. Twisk reports no competing interests; Prof. dr. J.F. de Boer has acquired grant support (for the institution; Department of Physics, VU) from the Dutch Research Council (NWO) and from industry (Thorlabs, ASML, Heidelberg Engineering). He has received royalties related to IP on OCT technologies and semiconductor metrology. He has acted as an expert witness for a UK based law firm; Prof. dr. P. Scheltens has received consultancy fees (paid to the university) from Alzheon, Brainstorm Cell and Green Valley. Within his university affiliation he is global PI of the phase 1b study of AC Immune, Phase 2b study with FUJI-film/Toyama and phase 2 study of UCB and phase 1 study with ImmunoBrain Checkpoint. He is chair of the EU steering committee of the phase 2b program of Vivoryon, the phase 2b study of Novartis Cardiology and co-chair of the phase 3 study with NOVO-Nordisk. He is also an employee of EQT Life Sciences (formerly LSP); Dr. B.D.C. Boon is supported by a research fellowship awarded by Alzheimer Nederland (#WE.15-2019-13); Prof. dr. D.R. Thal received speaker honorarium from Novartis Pharma Basel (Switzerland) and Biogen (USA), travel reimbursement from GE-Healthcare (UK), and UCB (Belgium), and collaborated with GE-Healthcare (UK), Novartis Pharma Basel (Switzerland), Probiodrug (Germany), and Janssen Pharmaceutical Companies (Belgium). He receives grants from Fonds Wetenschappelijk Onderzoek Vlaanderen (Belgium; FWO- G0F8516N, G065721N) and the Stichting Alzheimer Onderzoek (Belgium; SAO-FRA 2020/017); Prof. dr. A.J. Rozemuller reports no competing interests; Dr. F.D. Verbraak reports no competing interests; Dr. F. Bouwman performs contract research for Optina Dx and Optos, she has been an invited speaker at Roche and has been invited for expert testimony at Biogen. All funding is paid to her institution; Dr. J.J.M. Hoozemans received grants from the Dutch Research Council (ZonMW) and, Alzheimer Netherlands, performed contract research or received grants from Merck, ONO Pharmaceuticals, Janssen Prevention Center, DiscovericBio, AxonNeurosciences, Roche, Genentech, Promis, Denali, FirstBiotherapeutics, and Ensol Biosciences. All payments were made to the institution. Dr. J.J.M. Hoozemans participates in the scientific advisory board of Alzheimer Netherlands and is editor-in-chief for Acta Neuropathologica Communications.

References

1. Alafuzoff, I., P.G. Ince, T. Arzberger, S. Al-Sarraj, J. Bell, I. Bodi, et al., *Staging/typing of Lewy body related alpha-synuclein pathology: a study of the BrainNet Europe Consortium.* Acta Neuropathol, 2009. **117**(6): p. 635-52 https://doi.org/10.1007/s00401-009-0523-2.
2. Bankhead, P., M.B. Loughrey, J.A. Fernandez, Y. Dombrowski, D.G. McArt, P.D. Dunne, et al., *QuPath: Open source software for digital pathology image analysis.* Sci Rep, 2017. **7**(1): p. 16878 https://doi.org/10.1038/s41598-017-17204-5.
3. Boon, B.D.C., J.J.M. Hoozemans, B. Lopuhaa, K.N. Eigenhuis, P. Scheltens, W. Kamphorst, et al., *Neuroinflammation is increased in the parietal cortex of atypical Alzheimer's disease.* J Neuroinflammation, 2018. **15**(1): p. 170 https://doi.org/10.1186/s12974-018-1180-y.
4. Braak, H. and E. Braak, *Neuropathological stageing of Alzheimer-related changes.* Acta Neuropathol, 1991. **82**(4): p. 239-59 https://doi.org/10.1007/BF00308809.
5. Braak, H., I. Alafuzoff, T. Arzberger, H. Kretzschmar, and K. Del Tredici, *Staging of Alzheimer disease-associated neurofibrillary pathology using paraffin sections and immunocytochemistry.* Acta Neuropathol, 2006. **112**(4): p. 389-404 https://doi.org/10.1007/s00401-006-0127-z.
6. Bussiere, T., P.R. Hof, C. Mailliot, C.D. Brown, M.L. Caillet-Boudin, D.P. Perl, et al., *Phosphorylated serine422 on tau proteins is a pathological epitope found in several diseases with neurofibrillary degeneration.* Acta Neuropathol, 1999. **97**(3): p. 221-30 https://doi.org/10.1007/s004010050978.
7. Bussière, T., P.R. Hof, C. Mailliot, C.D. Brown, M.L. Caillet-Boudin, D.P. Perl, et al., *Phosphorylated serine422 on tau proteins is a pathological epitope found in several diseases with neurofibrillary degeneration.* Acta Neuropathologica, 1999. **97**(3): p. 221-230 https://doi.org/10.1007/s004010050978.
8. Chiasseu, M., L. Alarcon-Martinez, N. Belforte, H. Quintero, F. Dotigny, L. Destroismaisons, et al., *Tau accumulation in the retina promotes early neuronal dysfunction and precedes brain pathology in a mouse model of Alzheimer's disease.* Mol Neurodegener, 2017. **12**(1): p. 58 https://doi.org/10.1186/s13024-017-0199-3.
9. Chidlow, G., J.P. Wood, J. Manavis, J. Finnie, and R.J. Casson, *Investigations into Retinal Pathology in the Early Stages of a Mouse Model of Alzheimer's Disease.* J Alzheimers Dis, 2017. **56**(2): p. 655-675 https://doi.org/10.3233/JAD-160823.
10. Crary, J.F., J.Q. Trojanowski, J.A. Schneider, J.F. Abisambra, E.L. Abner, I. Alafuzoff, et al., *Primary age-related tauopathy (PART): a common pathology associated with human aging.* Acta Neuropathol, 2014. **128**(6): p. 755-66 https://doi.org/10.1007/s00401-014-1349-0.
11. de Silva, R., T. Lashley, C. Strand, A.M. Shiarli, J. Shi, J. Tian, et al., *An immunohistochemical study of cases of sporadic and inherited frontotemporal lobar degeneration using 3R- and 4R-specific tau monoclonal antibodies.* Acta Neuropathol, 2006. **111**(4): p. 329-40 https://doi.org/10.1007/s00401-006-0048-x.
12. den Haan, J., T.H.J. Morrema, F.D. Verbraak, J.F. de Boer, P. Scheltens, A.J. Rozemuller, et al., *Amyloid-beta and phosphorylated tau in post-mortem Alzheimer's disease retinas.* Acta Neuropathol Commun, 2018. **6**(1): p. 147 https://doi.org/10.1186/s40478-018-0650-x.
13. Dickson, D.W., C. Bergeron, S.S. Chin, C. Duyckaerts, D. Horoupian, K. Ikeda, et al., *Office of Rare Diseases neuropathologic criteria for corticobasal degeneration.* J Neuropathol Exp Neurol, 2002. **61**(11): p. 935-46 https://doi.org/10.1093/jnen/61.11.935.
14. Dowling, J.E., *Retina*, in *Encyclopedia of Human Biology*, L.R. Squire, Editor. 2009, Academic Press: New York.
15. Duyckaerts, C., H. Braak, J.P. Brion, L. Buee, K. Del Tredici, M. Goedert, et al., *PART is part of Alzheimer disease.* Acta Neuropathol, 2015. **129**(5): p. 749-56 https://doi.org/10.1007/s00401-015-1390-7.
16. Falcon, B., W. Zhang, A.G. Murzin, G. Murshudov, H.J. Garringer, R. Vidal, et al., *Structures of filaments from Pick's disease reveal a novel tau protein fold.* Nature, 2018. **561**(7721): p. 137-140 https://doi.org/10.1038/s41586-018-0454-y.
17. Furcila, D., J. DeFelipe, and L. Alonso-Nanclares, *A Study of Amyloid-beta and Phosphotau in Plaques and Neurons in the Hippocampus of Alzheimer's Disease Patients.* J Alzheimers Dis, 2018. **64**(2): p. 417-435 https://doi.org/10.3233/JAD-180173.
18. Grimaldi, A., N. Pediconi, F. Oieni, R. Pizzarelli, M. Rosito, M. Giubettini, et al., *Neuroinflammatory Processes, A1 Astrocyte Activation and Protein Aggregation in the Retina of Alzheimer's Disease Patients, Possible Biomarkers for Early Diagnosis.* Front Neurosci, 2019. **13**: p. 925 https://doi.org/10.3389/fnins.2019.00925.

19. Gupta, N., J. Fong, L.C. Ang, and Y.H. Yucel, *Retinal tau pathology in human glaucomas.* Can J Ophthalmol, 2008. **43**(1): p. 53-60 https://doi.org/10.3129/i07-185.
20. Hinton, D.R., A.A. Sadun, J.C. Blanks, and C.A. Miller, *Optic-nerve degeneration in Alzheimer's disease.* N Engl J Med, 1986. **315**(8): p. 485-7 https://doi.org/10.1056/nejm198608213150804.
21. Ho, C.Y., J.C. Troncoso, D. Knox, W. Stark, and C.G. Eberhart, *Beta-amyloid, phospho-tau and alpha-synuclein deposits similar to those in the brain are not identified in the eyes of Alzheimer's and Parkinson's disease patients.* Brain Pathol, 2014. **24**(1): p. 25-32 https://doi.org/10.1111/bpa.12070.
22. Ho, W.L., Y. Leung, S.S. Cheng, C.K. Lok, Y.S. Ho, L. Baum, et al., *Investigating degeneration of the retina in young and aged tau P301L mice.* Life Sci, 2015. **124**: p. 16-23 https://doi.org/10.1016/j.lfs.2014.12.019.
23. Hyman, B.T., C.H. Phelps, T.G. Beach, E.H. Bigio, N.J. Cairns, M.C. Carrillo, et al., *National Institute on Aging-Alzheimer's Association guidelines for the neuropathologic assessment of Alzheimer's disease.* Alzheimers Dement, 2012. **8**(1): p. 1-13 https://doi.org/10.1016/j.jalz.2011.10.007.
24. Iacono, D., P. Lee, B.L. Edlow, N. Gray, B. Fischl, K. Kenney, et al., *Early-Onset Dementia in War Veterans: Brain Polypathology and Clinicopathologic Complexity.* J Neuropathol Exp Neurol, 2020. **79**(2): p. 144-162 https://doi.org/10.1093/jnen/nlz122.
25. Jellinger, K.A., *Multiple System Atrophy: An Oligodendroglioneural Synucleinopathy1.* J Alzheimers Dis, 2018. **62**(3): p. 1141-1179 https://doi.org/10.3233/JAD-170397.
26. Kaur, C., W.S. Foulds, and E.A. Ling, *Blood-retinal barrier in hypoxic ischaemic conditions: basic concepts, clinical features and management.* Prog Retin Eye Res, 2008. **27**(6): p. 622-47 https://doi.org/10.1016/j.preteyeres.2008.09.003.
27. Klioueva, N.M., M.C. Rademaker, D.T. Dexter, S. Al-Sarraj, D. Seilhean, N. Streichenberger, et al., *BrainNet Europe's Code of Conduct for brain banking.* J Neural Transm (Vienna), 2015. **122**(7): p. 937-40 https://doi.org/10.1007/s00702-014-1353-5.
28. Koronyo-Hamaoui, M., Y. Koronyo, A.V. Ljubimov, C.A. Miller, M.K. Ko, K.L. Black, et al., *Identification of amyloid plaques in retinas from Alzheimer's patients and noninvasive in vivo optical imaging of retinal plaques in a mouse model.* Neuroimage, 2011. **54 Suppl 1**: p. S204-17 https://doi.org/10.1016/j.neuroimage.2010.06.020.
29. Kovacs, G.G., I. Ferrer, L.T. Grinberg, I. Alafuzoff, J. Attems, H. Budka, et al., *Aging-related tau astrogliopathy (ARTAG): harmonized evaluation strategy.* Acta Neuropathol, 2016. **131**(1): p. 87-102 https://doi.org/10.1007/s00401-015-1509-x.
30. Leger, F., P.O. Fernagut, M.H. Canron, S. Leoni, C. Vital, F. Tison, et al., *Protein aggregation in the aging retina.* J Neuropathol Exp Neurol, 2011. **70**(1): p. 63-8 https://doi.org/10.1097/NEN.0b013e31820376cc.
31. Loffler, K.U., D.P. Edward, and M.O. Tso, *Immunoreactivity against tau, amyloid precursor protein, and beta-amyloid in the human retina.* Invest Ophthalmol Vis Sci, 1995. **36**(1): p. 24-31.
32. London, A., I. Benhar, and M. Schwartz, *The retina as a window to the brain-from eye research to CNS disorders.* Nat Rev Neurol, 2013. **9**(1): p. 44-53 https://doi.org/10.1038/nrneurol.2012.227.
33. McKeith, I.G., B.F. Boeve, D.W. Dickson, G. Halliday, J.P. Taylor, D. Weintraub, et al., *Diagnosis and management of dementia with Lewy bodies: Fourth consensus report of the DLB Consortium.* Neurology, 2017. **89**(1): p. 88-100 https://doi.org/10.1212/WNL.0000000000004058.
34. McMillan, P.J., T.J. Strovas, M. Baum, B.K. Mitchell, R.J. Eck, N. Hendricks, et al., *Pathological tau drives ectopic nuclear speckle scaffold protein SRRM2 accumulation in neuron cytoplasm in Alzheimer's disease.* Acta Neuropathol Commun, 2021. **9**(1): p. 117 https://doi.org/10.1186/s40478-021-01219-1.
35. Mirra, S.S., A. Heyman, D. McKeel, S.M. Sumi, B.J. Crain, L.M. Brownlee, et al., *The Consortium to Establish a Registry for Alzheimer's Disease (CERAD). Part II. Standardization of the neuropathologic assessment of Alzheimer's disease.* Neurology, 1991. **41**(4): p. 479-86 https://doi.org/10.1212/wnl.41.4.479.
36. Ossenkoppele, R., R. van der Kant, and O. Hansson, *Tau biomarkers in Alzheimer's disease: towards implementation in clinical practice and trials.* The Lancet Neurology, 2022 https://doi.org/https://doi.org/10.1016/S1474-4422(22)00168-5.
37. Ozaki, K., T. Irioka, T. Uchihara, A. Yamada, A. Nakamura, T. Majima, et al., *Neuropathology of SCA34 showing widespread oligodendroglial pathology with vacuolar white matter*

degeneration: a case study. Acta Neuropathol Commun, 2021. **9**(1): p. 172 https://doi.org/10.1186/s40478-021-01272-w.
38. Pasteels, B., J. Rogers, F. Blachier, and R. Pochet, *Calbindin and calretinin localization in retina from different species.* Vis Neurosci, 1990. **5**(1): p. 1-16 https://doi.org/10.1017/s0952523800000031.
39. Regalado-Reyes, M., D. Furcila, F. Hernandez, J. Avila, J. DeFelipe, and G. Leon-Espinosa, *Phospho-Tau Changes in the Human CA1 During Alzheimer's Disease Progression.* J Alzheimers Dis, 2019. **69**(1): p. 277-288 https://doi.org/10.3233/JAD-181263.
40. Schon, C., N.A. Hoffmann, S.M. Ochs, S. Burgold, S. Filser, S. Steinbach, et al., *Long-term in vivo imaging of fibrillar tau in the retina of P301S transgenic mice.* PLoS One, 2012. **7**(12): p. e53547 https://doi.org/10.1371/journal.pone.0053547.
41. Snyder, P.J., J. Alber, C. Alt, L.J. Bain, B.E. Bouma, F.H. Bouwman, et al., *Retinal imaging in Alzheimer's and neurodegenerative diseases.* Alzheimers Dement, 2021. **17**(1): p. 103-111 https://doi.org/10.1002/alz.12179.
42. Taylor, A.W. and J.W. Streilein, *Inhibition of antigen-stimulated effector T cells by human cerebrospinal fluid.* Neuroimmunomodulation, 1996. **3**(2-3): p. 112-8 https://doi.org/10.1159/000097235.
43. Thal, D.R., U. Rub, M. Orantes, and H. Braak, *Phases of A beta-deposition in the human brain and its relevance for the development of AD.* Neurology, 2002. **58**(12): p. 1791-800 https://doi.org/10.1212/wnl.58.12.1791.
44. Wennstrom, M., S. Janelidze, K.P.R. Nilsson, B. Netherlands Brain, G.E. Serrano, T.G. Beach, et al., *Cellular localization of p-tau217 in brain and its association with p-tau217 plasma levels.* Acta Neuropathol Commun, 2022. **10**(1): p. 3 https://doi.org/10.1186/s40478-021-01307-2.
45. Wilbanks, G.A. and J.W. Streilein, *Fluids from immune privileged sites endow macrophages with the capacity to induce antigen-specific immune deviation via a mechanism involving transforming growth factor-beta.* Eur J Immunol, 1992. **22**(4): p. 1031-6 https://doi.org/10.1002/eji.1830220423.
46. Williams, E.A., D. McGuone, M.P. Frosch, B.T. Hyman, N. Laver, and A. Stemmer-Rachamimov, *Absence of Alzheimer Disease Neuropathologic Changes in Eyes of Subjects With Alzheimer Disease.* J Neuropathol Exp Neurol, 2017. **76**(5): p. 376-383 https://doi.org/10.1093/jnen/nlx020.
47. Yan, W., Y.R. Peng, T. van Zyl, A. Regev, K. Shekhar, D. Juric, et al., *Cell Atlas of The Human Fovea and Peripheral Retina.* Sci Rep, 2020. **10**(1): p. 9802 https://doi.org/10.1038/s41598-020-66092-9.
48. Zhang, W., A. Tarutani, K.L. Newell, A.G. Murzin, T. Matsubara, B. Falcon, et al., *Novel tau filament fold in corticobasal degeneration.* Nature, 2020. **580**(7802): p. 283-287 https://doi.org/10.1038/s41586-020-2043-0.

Tables and figure legends

Table 1 Characteristics of post mortem brain and eye tissue used in this study. Age at death is shown in years.

Table 2 Primary antibodies used in this study.

Table 3 Group demographics of cases used in this study.
Data are shown as mean ± SD or median and interquartile range (IQR); Age at death is shown in years. The post-mortem interval of eyes is shown in hours.

Table 4 Cases assessed for tau pathology in the visual system.

Table 5 Results of the statistical analysis with a linear mixed model to study the difference between controls with Braak stage 0 and other groups.
For total tau mean surface %, a total of 103 datapoints was available for analysis (60 cases, 22 missing values), for p-tau Ser202/Thr205 mean surface %, a total of 116 datapoints was available for analysis (62 cases, 8 missing values), for p-tau Thr217 mean surface % 111 datapoints (58 cases, 13 missing values), for p-tau Thr212/Ser214 mean surface % 98 datapoints (56 cases, 14 missing values), for p-tau Thr181 mean surface % 91 datapoints (55 cases, 19 missing values), and for p-tau Ser396 mean surface % 109 datapoints (57 cases, 14 missing values).

Figure 1 Illustration of the tau protein with phospho-epitopes assessed.
This visual representation of the tau protein depicts the epitopes (black) and their primary antibodies (gray) used for immunohistochemistry to study tau and p-tau in the retina.

Figure 2 Total tau, tau isoforms and phosphorylated tau in the medial frontal gyrus of different groups.
Total tau (HT7), 3R and 4R tau isoforms, and different phospho-epitopes of tau were assessed using immunohistochemistry on the medial frontal gyrus. Shown are representative cases from all different groups: control Braak stage 0, control Braak stage I-III, Alzheimer's disease, Progressive supranuclear palsy, Frontotemporal lobar degeneration-TDP and Parkinson's disease.
Scale bar: 100 µm (applicable to all images). Immunostaining shown with DAB (brown) and nuclei are counterstained with hematoxylin (blue).

Figure 3 Total tau, tau isoforms and tau phospho-epitopes in the retinas of different groups.
Total tau (HT7), 3R and 4R tau isoforms, and different phospho-epitopes of tau were assessed using immunohistochemistry on the far periphery of the superior retina. Shown are representative cases from all different groups: control Braak stage 0, control Braak stage I-III, Alzheimer's disease, Progressive supranuclear palsy, Frontotemporal lobar degeneration-TDP and Parkinson's disease.
Scale bar: 50 µm (applicable to all images). Immunostaining shown with DAB (brown) and nuclei are counterstained with hematoxylin (blue).

Figure 4 Localization of p-tau in the retina.

a Total tau assessed with HT7 is present in the IPL and the OPL (control case, #1). **b** Detection of p-tau Thr181 in a cross-section of the retina shows the different retinal layers and the different anatomical sublaminar layers of the IPL (AD case, #16). **c** A schematic overview of the retinal layers, including the retinal neuronal cells. **d** Intracellular p-tau assessed with p-tau Ser202/Thr205 was observed localized in the INL with branching extended in the OPL of the retina (primary tauopathy, case #39). **e** Immunostaining with p-tau Ser202/Thr205 reveals a prominent localization of p-tau in the far periphery as opposed to the mid periphery and central region. The box-plot shows the distribution of the mean surface % of p-tau Ser202/Thr205 immunoreactivity (n=62) in the far periphery, mid periphery and central region. **f** Some cases show a different distribution of p-tau presence in the IPL and OPL. Shown are examples of p-tau Ser202/Thr205 and Thr217 present in the IPL in CBD (#33), whereas the PSP case (#35) mainly shows immunoreactivity in the OPL. Total tau (HT7) in these cases is present in both the IPL and OPL.

Scale bar: 50 µm (applicable to all images). Immunostaining shown with DAB (brown) and nuclei are counterstained with hematoxylin (blue). Abbreviations: CBD, corticobasal degeneration; PSP, progressive supranuclear palsy. Statistical analysis was performed using linear mixed model; **P* value < 0.001.

Figure 5 Fluorescent double-immunostainings for total tau, p-tau Ser202/Thr205 and p-tau Thr217 with calbindin D28K and calretinin.

Shown from top to bottom are fluorescent double-immunostainings of calbindin D28K and calretinin with total tau (a, b), p-tau Ser202/Thr205 (c, d) and p-tau Thr217 (e, f) on the far periphery of the superior part retina. **a, c, e** Calbindin D28K (red) is detected in cones, horizontal cells and bipolar cells. Colocalization of total tau (a) p-tau Ser202/Thr205 (c) and Thr217 (e) with calbindin D28K is observed in what presumably are horizontal cells in the INL (yellow). **b, d, f** Calretinin (red) is detected in amacrine cells in the INL and their processes in the IPL. Fluorescent double-immunostaining for total tau (b), p-tau Ser202/Thr205 (d) and calretinin (f) revealed colocalization of p-tau with amacrine cells (yellow).

Scale bar: 50 µm (applicable to all images). Nuclear staining with DAPI (blue). Abbreviations: INL, inner nuclear layer.

Figure 6 Total tau and p-tau levels in the far and mid periphery of the superior retina.

Shown are the overall differences between groups for total tau (a), p-tau Ser202/Thr205 (b), p-tau Thr217 (c), p-tau Thr212/Ser214 (d), p-tau Thr181 (e) and p-tau Ser396 (f) in the far periphery (dark green) and mid periphery (light green) of the superior retina. Groups consist of control cases without tau pathology (Braak 0) or low-moderate tau pathology (Braak I-III), Alzheimer's disease cases (AD), primary tauopathies (Tauopathies), other neurodegenerative diseases (OND), or α-synucleinopathies (α-syn). Immunoreactivity was quantified as mean surface % area immunoreactivity in the far and mid periphery of the retina. Violin plots depict the median (solid line) and inter quartile range (dashed line) of all cases (n=62). Abbreviations: AD, Alzheimer's disease; OND, other neurodegenerative diseases;

α-syn, α-synucleinopathies. Statistical analysis was performed using linear mixed model; *P value < 0.05; **P value < 0.005; ***P value < 0.001.

Figure 7 Relation between retinal p-tau immunoreactivity and cerebral cortical p-tau among different brain regions.
Shown is the mean surface % area immunoreactivity in the far periphery of the superior retina for all cases (n=62) for p-tau Ser202/Thr205 and p-tau Thr217 along the scores for p-tau load in the brain. Scores for brain p-tau load Ser202/Thr205 or Thr217 are depicted as follows; -, none; +, few; ++, moderate; +++, high (for score examples see supplementary fig. 3, online resource). P-tau in the retina was compared with p-tau load in the hippocampus (a,b), temporal pole (c,d), medial frontal gyrus (e,f), inferior parietal lobe (g,h), and occipital pole (i,j). The violin plots depict the median (solid line) and inter quartile range (dashed line) of all cases (n=62).

Figure 8 Patterns of p-tau Ser202/Thr205 immunoreactivity in the visual system.
Shown are different regions of the visual system of three AD cases with Braak stage V or VI: from left to right the far periphery superior retina (a, e, i), superior colliculus (b, f, j), LGN (c, g, k) and occipital pole (d, h, l) are shown. **a-d** AD case (#29) showing no p-tau Ser202/Thr205 immunoreactivity in the retina (a), mild to moderate p-tau Ser202/Thr205 load in the superior colliculus (b) and LGN (c) and high p-tau Ser202/Thr205 load in the occipital pole (d). **e-h** AD case (#25) showing moderate p-tau Ser202/Thr205 immunoreactivity in the retina, and mild p-tau Ser202/Thr205 presence in the superior colliculus (f), LGN (g) and occipital pole (h). **i-l** AD case (#28) showing a relatively high presence of p-tau Ser202/Thr205 in the far periphery of the retina, and mild to high p-tau Ser202/Thr205 immunoreactivity in the superior colliculus (j), LGN (k) and occipital pole (l).
Scale bar: 50 µm (applicable to all images). Immunostaining shown with DAB (brown) and nuclei are counterstained with hematoxylin (blue).

Supplementary figure 1 Threshold determination of DAB positive surface area for p-tau Ser202/Thr205 immunoreactivity
a The best fitting threshold for each immunostaining was determined by assessing the spread of mean surface % datapoints using a scatter dot plot. **b** In Qupath, the best fitting threshold derived from the scatter dot plot was reviewed to verify accurate inclusion of DAB positive surface area (in red) within the ROI (in yellow). For p-tau Ser202/Thr205 a threshold of 0.2 optical density units was chosen as best fitting the accurate inclusion of immunopositivity.

Supplementary figure 2 Score examples for p-tau Ser202/Thr205 immunoreactivity in the brain.
Mid-hippocampal region is depicted and semi-quantitatively scored as none (a), few (b), moderate (c) and high (d). Scale bar represents 50µm (applicable for all images). Immunostaining shown with DAB (brown) and nuclei are counterstained with hematoxylin (blue).

Supplementary figure 3 Distribution of p-tau in the retina.

Immunoreactivity for tau and p-tau was assessed in the superior retina in the far periphery, mid periphery and central region.

a Analysis with a linear mixed model indicates that the immunoreactivity levels of total tau, p-tau Ser202/Thr205, Thr217, Thr212/Ser214, Thr181 and Ser396 are significantly increased in the far peripheral region compared with mid periphery and central region (n=62). As the far peripheral region is used as a reference variable, it is not shown in the table. **b** Boxplots show the distribution of the average values of all cases (n=62) for total tau, p-tau Ser202/Thr205, Thr217, Thr212/Ser214, Thr181 and Ser396. Statistical analysis was performed using linear mixed model; *P value < 0.001.

Supplementary figure 4 Signals after omission of primary antibody. DAPI signal is shown for reference. Filter cube wavelengths (excitation/emission) are depicted in the figure per dye: DAPI (excitation: 325-375; emission: 435-485), FITC (excitation: 460-500; emission: 512-542) and Texas-red (excitation: 540-580; emission: 592-668).

Figure 1

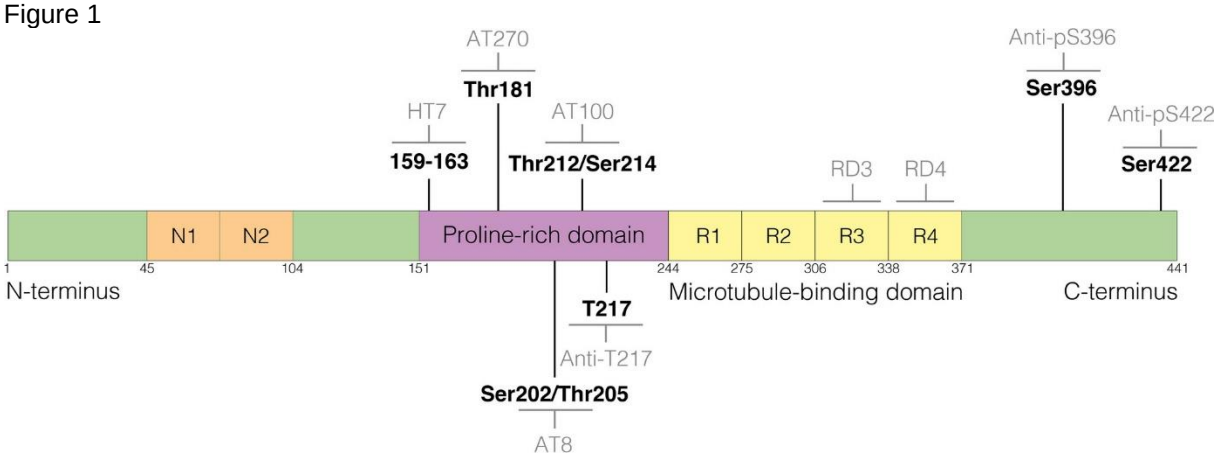
AT270
Thr181
HT7
159-163
AT100
Thr212/Ser214
Anti-pS396
Ser396
Anti-pS422
Ser422
RD3
RD4
N1
N2
Proline-rich domain
R1
R2
R3
R4
1
45
104
151
244
275
306
338
371
441
N-terminus
Microtubule-binding domain
C-terminus
T217
Anti-T217
Ser202/Thr205
AT8

Figure 2

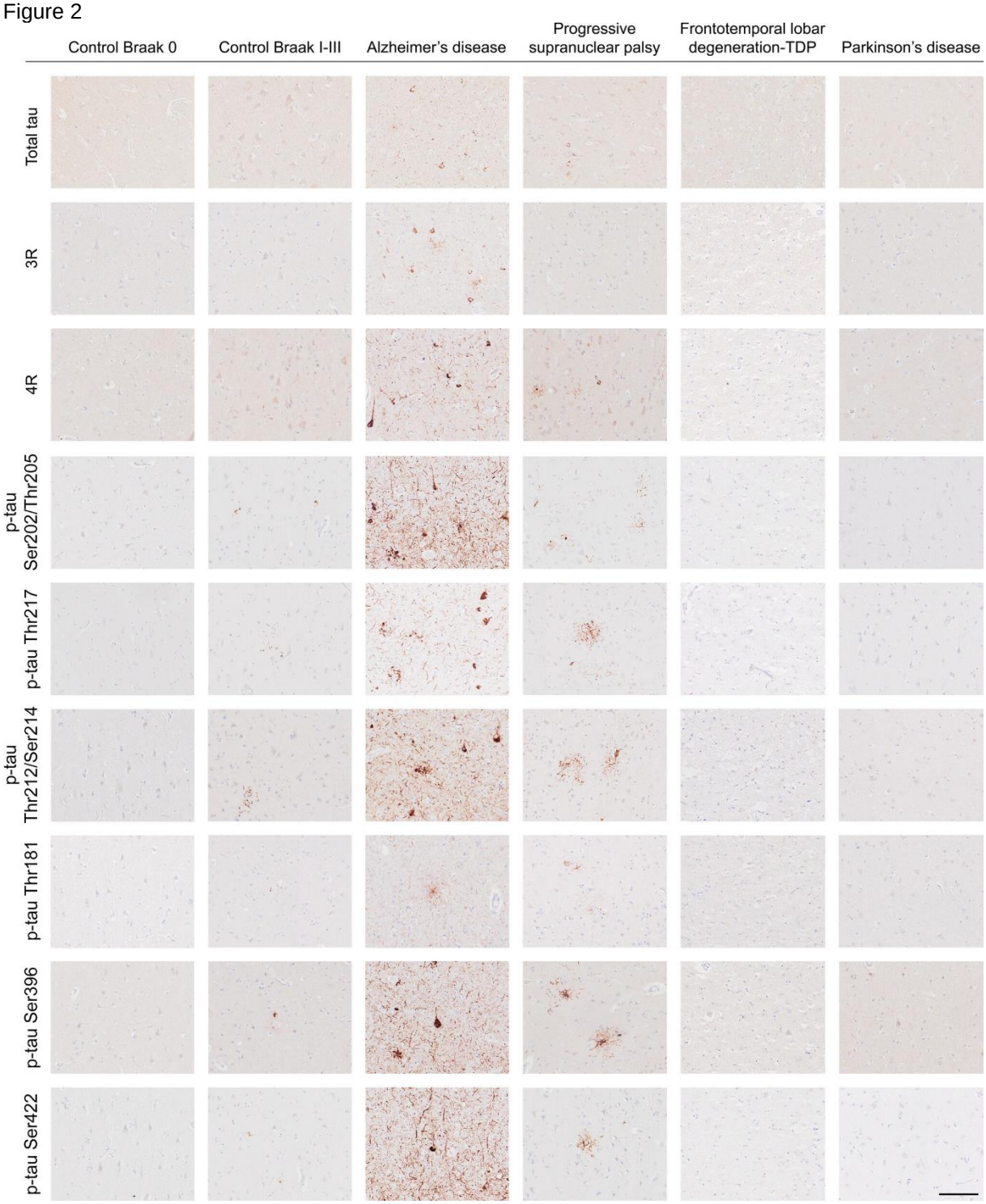
Control Braak 0
Control Braak I-III
Alzheimer's disease
Progressive supranuclear palsy
Frontotemporal lobar degeneration-TDP
Parkinson's disease
Total tau
3R
4R
p-tau Ser202/Thr205
p-tau Thr217
p-tau Thr212/Ser214
p-tau Thr181
p-tau Ser396
p-tau Ser422

Figure 3

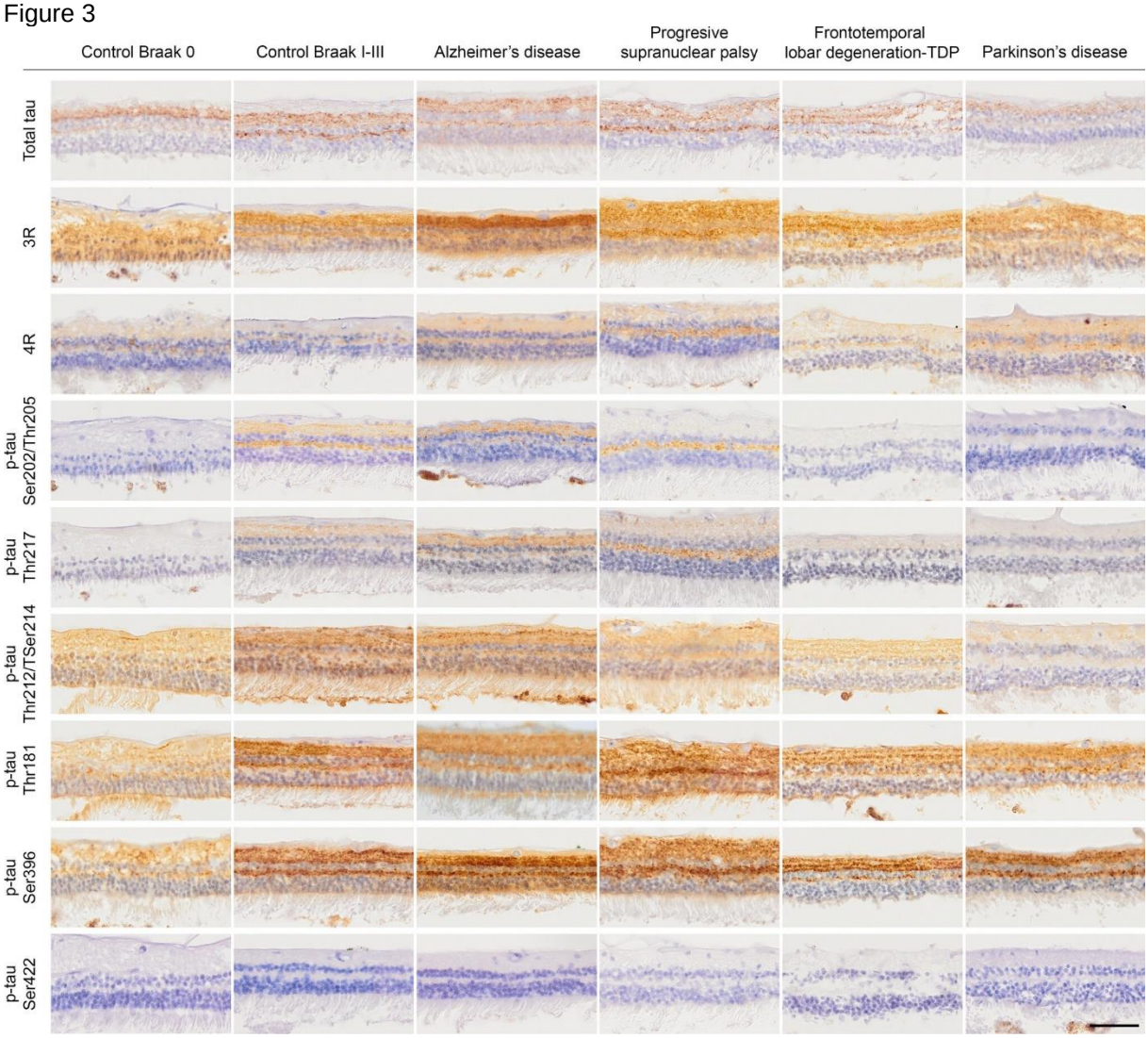
Control Braak 0
Control Braak I-III
Alzheimer's disease
Progresive supranuclear palsy
Frontotemporal lobar degeneration-TDP
Parkinson's disease
Total tau
3R
4R
p-tau Ser202/Thr205
p-tau Thr217
p-tau Thr212/TSer214
p-tau Thr181
p-tau Ser396
p-tau Ser422

Figure 4

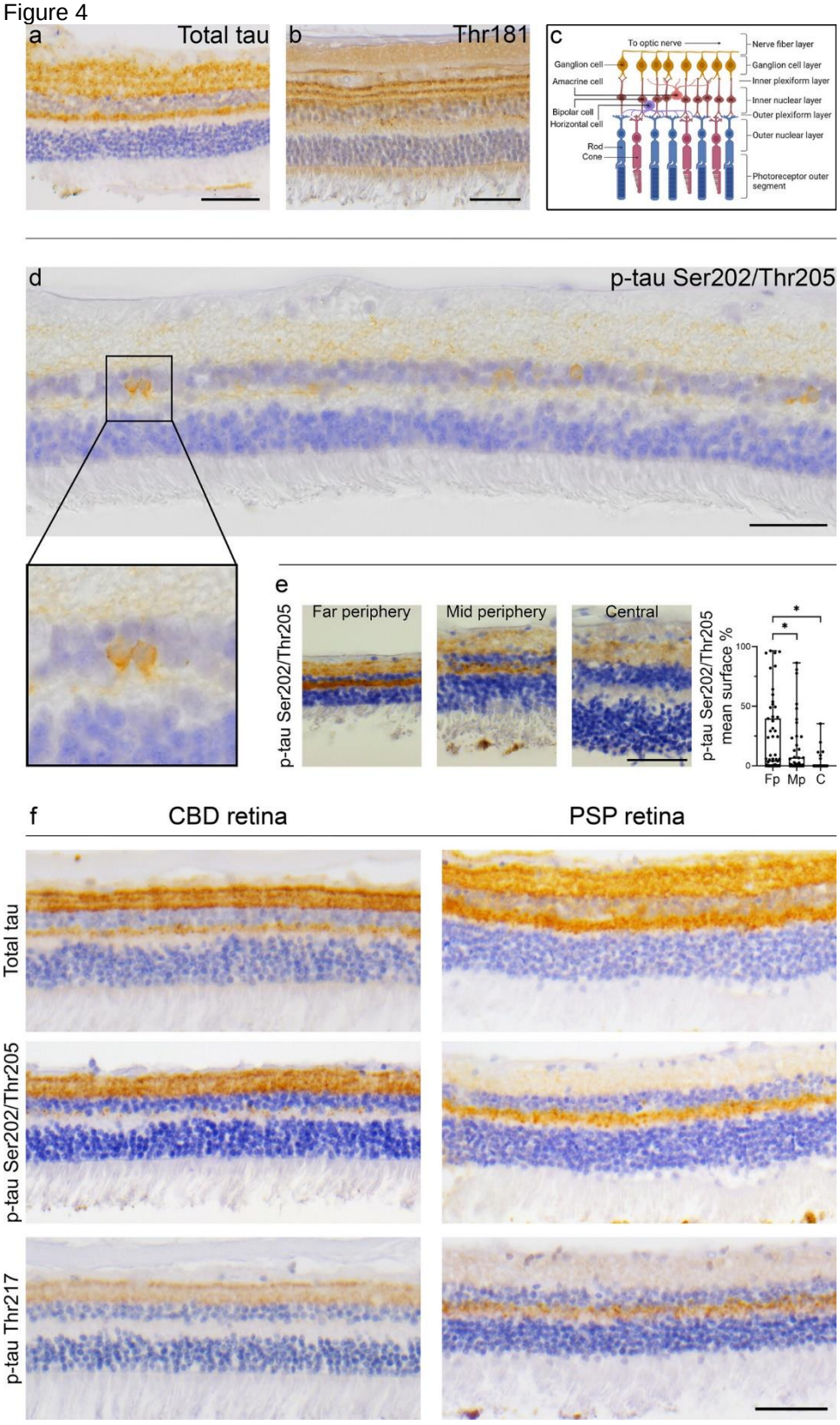
a
Total tau
b
Thr181
c
To optic nerve
Ganglion cell
Amacrine cell
Bipolar cell
Horizontal cell
Rod
Cone
Nerve fiber layer
Ganglion cell layer
Inner plexiform layer
Inner nuclear layer
Outer plexiform layer
Outer nuclear layer
Photoreceptor outer segment
d
p-tau Ser202/Thr205
e
p-tau Ser202/Thr205
Far periphery
Mid periphery
Central
p-tau Ser202/Thr205 mean surface %
100
50
0
Fp
Mp
C
*
*
f
CBD retina
PSP retina
Total tau
p-tau Ser202/Thr205
p-tau Thr217

Figure 5

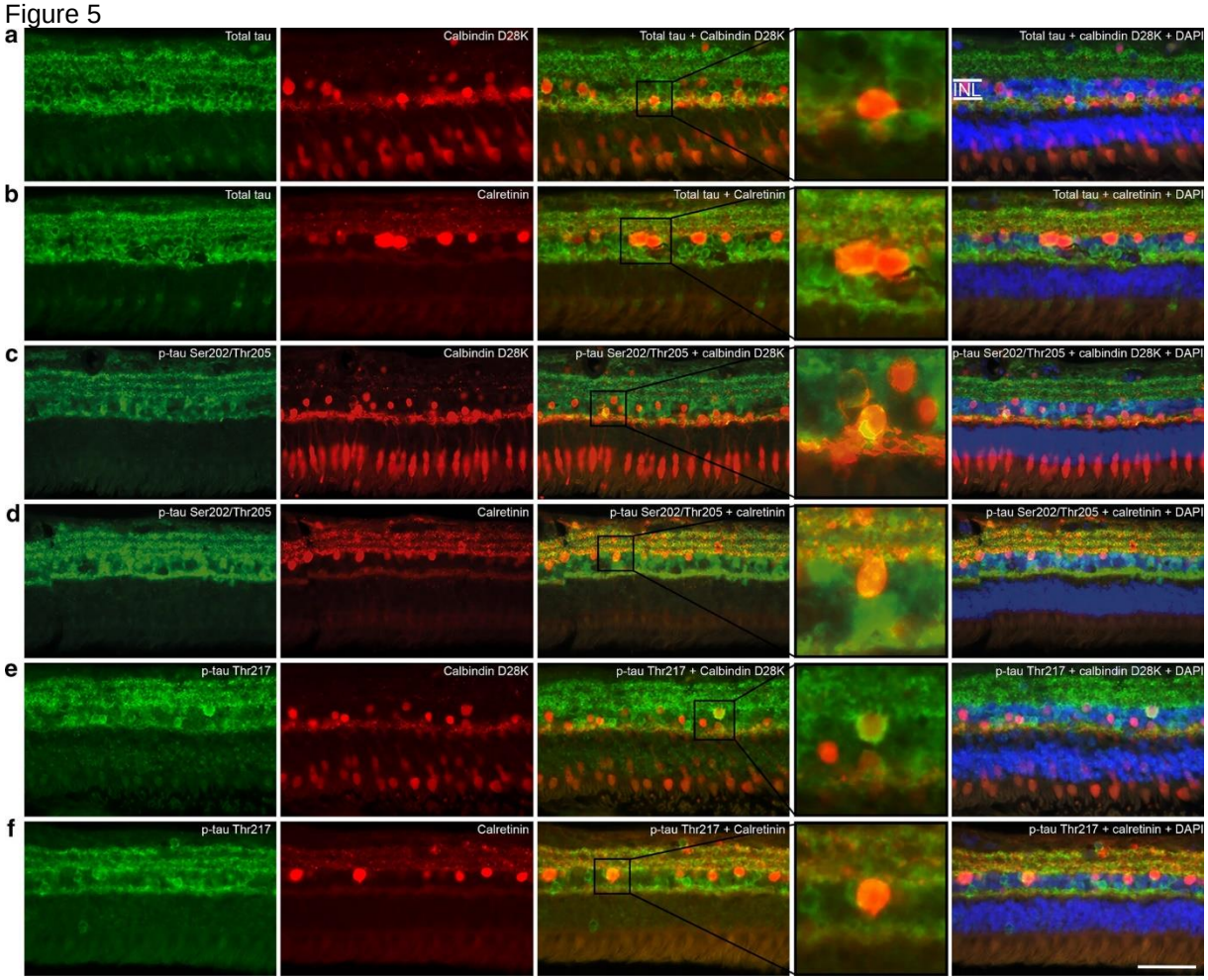
a
Total tau
Calbindin D28K
Total tau + Calbindin D28K
Total tau + calbindin D28K + DAPI
INL
b
Total tau
Calretinin
Total tau + Calretinin
Total tau + calretinin + DAPI
c
p-tau Ser202/Thr205
Calbindin D28K
p-tau Ser202/Thr205 + calbindin D28K
p-tau Ser202/Thr205 + calbindin D28K + DAPI
d
p-tau Ser202/Thr205
Calretinin
p-tau Ser202/Thr205 + calretinin
p-tau Ser202/Thr205 + calretinin + DAPI
e
p-tau Thr217
Calbindin D28K
p-tau Thr217 + Calbindin D28K
p-tau Thr217 + calbindin D28K + DAPI
f
p-tau Thr217
Calretinin
p-tau Thr217 + Calretinin
p-tau Thr217 + calretinin + DAPI

Figure 6

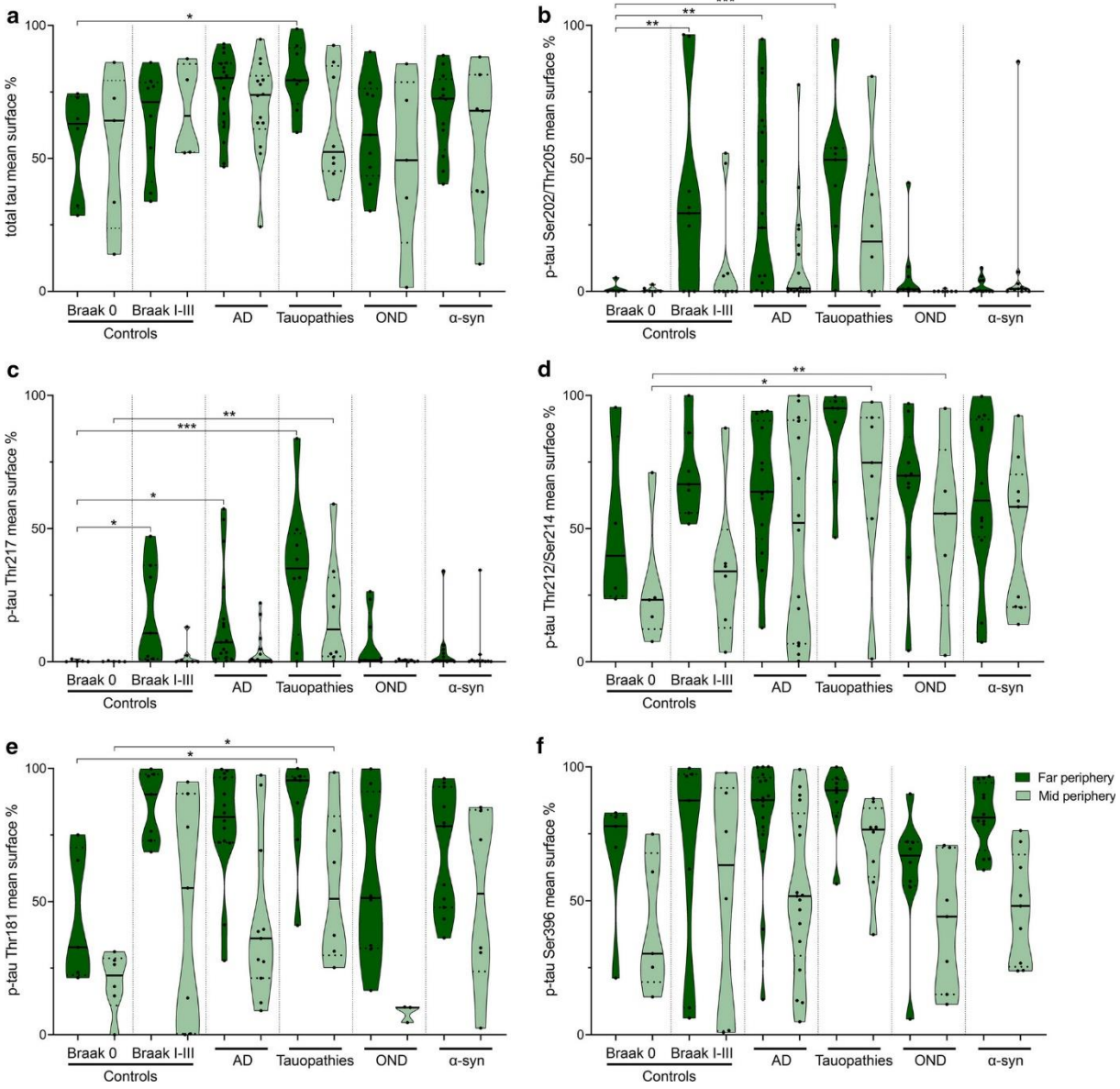
a
total tau mean surface %
b
p-tau Ser202/Thr205 mean surface %
c
p-tau Thr217 mean surface %
d
p-tau Thr212/Ser214 mean surface %
e
p-tau Thr181 mean surface %
f
p-tau Ser396 mean surface %
Far periphery
Mid periphery
Braak 0
Braak I-III
Controls
AD
Tauopathies
OND
α-syn

Figure 7

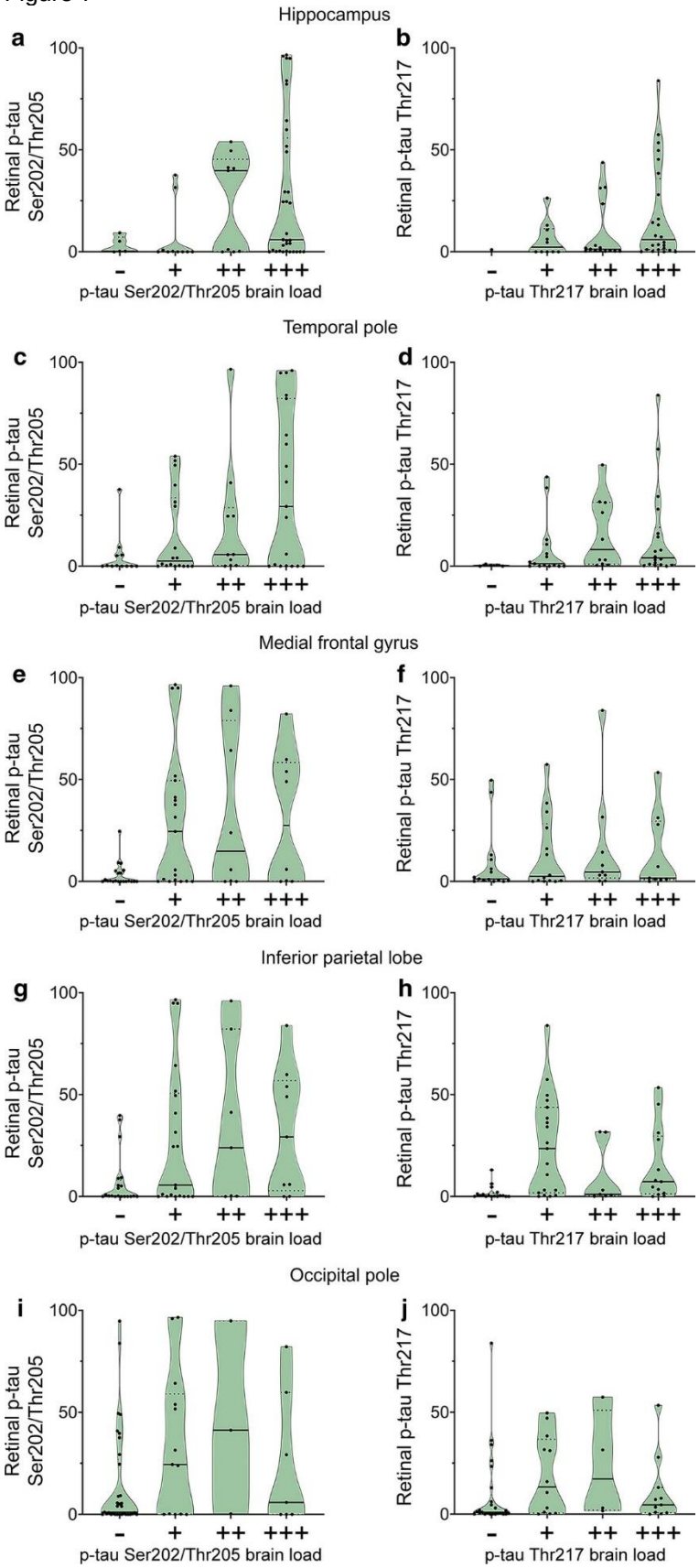
Hippocampus
a
b
Retinal p-tau Ser202/Thr205
Retinal p-tau Thr217
100
50
0
– + ++ +++
p-tau Ser202/Thr205 brain load
p-tau Thr217 brain load
Temporal pole
c
d
Medial frontal gyrus
e
f
Inferior parietal lobe
g
h
Occipital pole
i
j

Figure 8

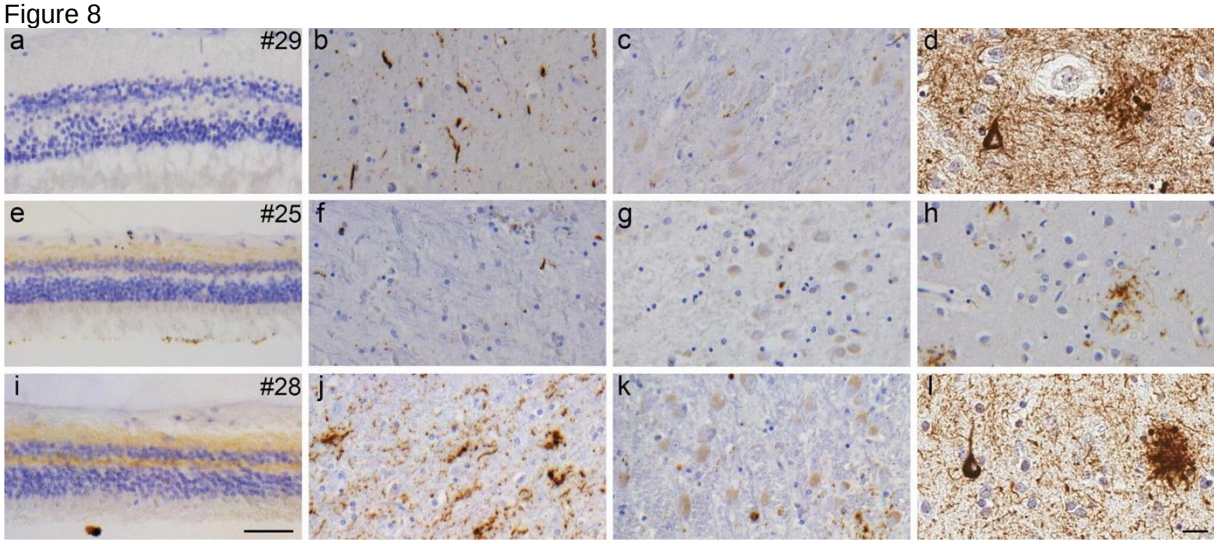

Phosphorylated tau in the retina correlates with tau pathology in the brain in Alzheimer's disease and primary tauopathies (Acta Neuropathologica)

Frederique J. Hart de Ruyter[1,2], Tjado H.J. Morrema[1], Jurre den Haan[2], Netherlands Brain Bank[3], Jos W.R. Twisk[4], Johannes F. de Boer[5], Philip Scheltens[2], Baayla D.C. Boon[1,2,6], Dietmar R. Thal[7], Annemieke J. Rozemuller[1], Frank D. Verbraak[8], Femke H. Bouwman[2,9], Jeroen J.M. Hoozemans[1,9]

1 Amsterdam UMC location Vrije Universiteit Amsterdam, Pathology, Amsterdam, De Boelelaan 1117, Amsterdam, The Netherlands
2 Alzheimer Center Amsterdam, Neurology, Vrije Universiteit Amsterdam, Amsterdam UMC location VUmc, Amsterdam, The Netherlands
3 Netherlands Institute for Neuroscience, Meibergdreef 47, 1105 BA, Amsterdam, the Netherlands
4 Amsterdam UMC location Vrije Universiteit Amsterdam, Epidemiology and Data Science, Amsterdam, De Boelelaan 1117, Amsterdam, The Netherlands
5 Vrije Universiteit Amsterdam, LaserLaB, Physics and Astronomy, Amsterdam, The Netherlands
6 Mayo Clinic, Neuroscience, Jacksonville, Florida, USA
7 KU Leuven, Leuven Brain Institute, 3000 Leuven, Belgium; Laboratory for Neuropathology, Department of Imaging and Pathology, KU Leuven, and Department of Pathology, UZ Leuven, 3000 Leuven, Belgium
8 Amsterdam UMC location Vrije Universiteit Amsterdam, Ophthalmology, Amsterdam, De Boelelaan 1117, Amsterdam, The Netherlands
9 Amsterdam Neuroscience, Neurodegeneration, Amsterdam, the Netherlands

Corresponding author:

Jeroen J.M. Hoozemans, jjm.hoozemans@amsterdamumc.nl, +31204444444

Frederique J. Hart de Ruyter, f.hartderuijter@amsterdamumc.nl, +31204440912

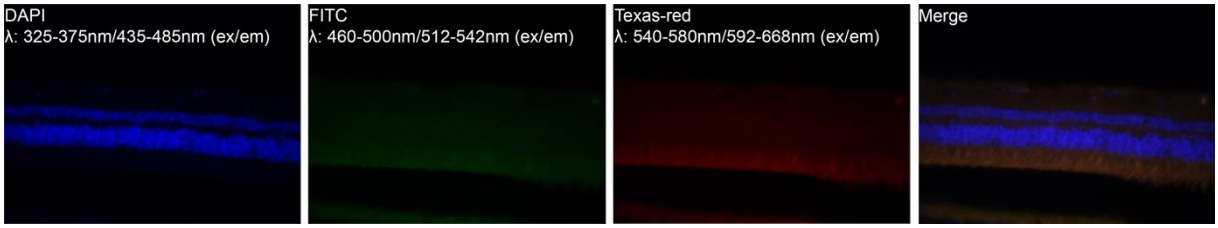

Supplementary Figure 1 Signals after omission of primary antibody. DAPI signal is shown for reference. Filter cube wavelengths (excitation/emission) are depicted in the figure per dye: DAPI (excitation: 325-375; emission: 435-485), FITC (excitation: 460-500; emission: 512-542) and Texas-red (excitation: 540-580; emission: 592-668).

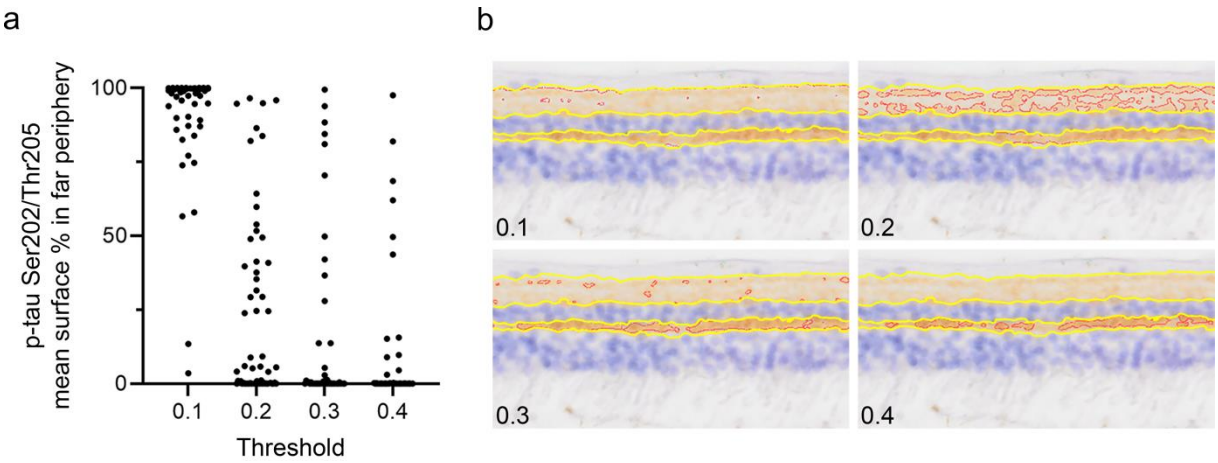

Supplementary Figure 2 Threshold determination of DAB positive surface area for p-tau Ser202/Thr205 immunoreactivity.

a The best fitting threshold for each immunostaining was determined by assessing the spread of mean surface % datapoints using a scatter dot plot. **b** In Qupath, the best fitting threshold derived from the scatter dot plot was reviewed to verify accurate inclusion of DAB positive surface area (in red) within the ROI (in yellow). For p-tau Ser202/Thr205 a threshold of 0.2 was chosen as best fitting the accurate inclusion of immunopositivity.

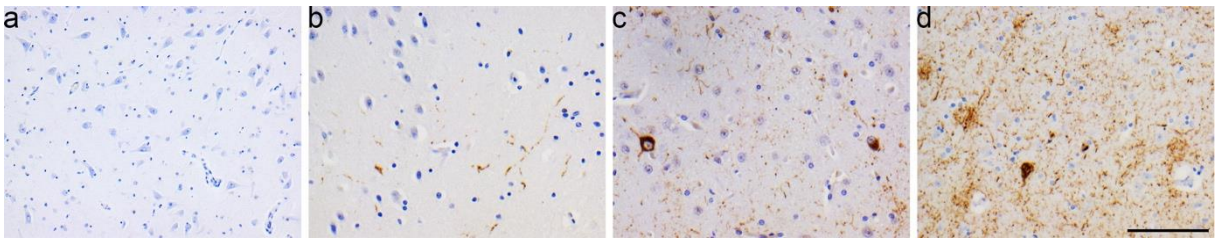

Supplementary Figure 3 Score examples for p-tau Ser202/Thr205 immunoreactivity in the brain. Mid-hippocampal region is depicted and semi-quantitatively scored as none (a), few (b), moderate (c) and high (d). Scale bar represents 50µm (applicable for all images). Immunostaining shown with DAB (brown) and nuclei are counterstained with hematoxylin (blue).

a

P-tau epitope	Retinal region	Coefficient	SE	*P* value	[95% CI]	
Total tau	Mid periphery	-8.28	3.13	<0.001*	-14.42	-2.14
	Central	-46.93	3.34	<0.001*	-53.48	-40.36
Ser202/Thr205	Mid periphery	-11.76	1.28	<0.001*	-14.28	-9.24
	Central	-21.92	1.44	<0.001*	-24.73	-19.10
Thr217	Mid periphery	-8.48	0.74	<0.001*	-9.93	-7.02
	Central	-13.22	0.74	<0.001*	-14.67	-11.78
Thr212/Ser214	Mid periphery	-16.76	1.63	<0.001*	-19.95	-13.57
	Central	-49.71	2.03	<0.001*	-53.69	-45.73
Thr181	Mid periphery	-31.34	1.43	<0.001*	-34.13	-28.55
	Central	-65.08	1.68	<0.001*	-68.38	-61.78
Ser396	Mid periphery	-24.50	1.30	<0.001*	-27.05	-21.94
	Central	-49.97	1.34	<0.001*	-52.60	-47.34

b

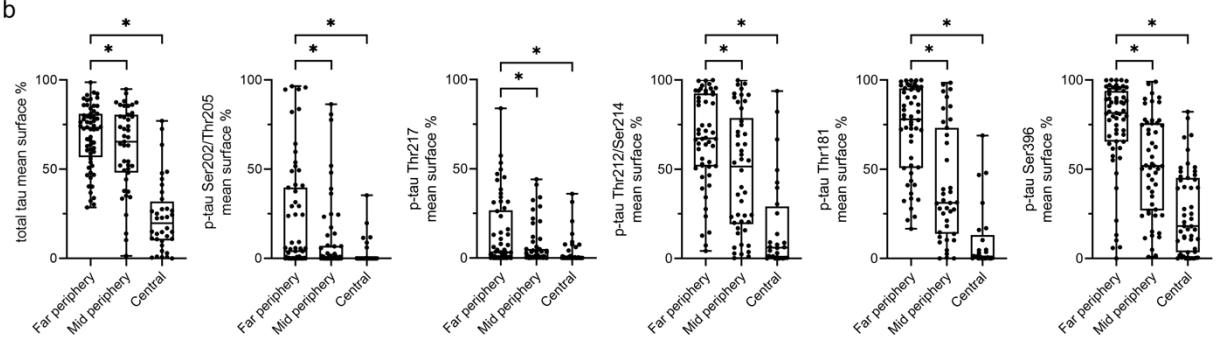

Supplementary Figure 4 Distribution of p-tau in the retina.

Immunoreactivity for tau and p-tau was assessed in the superior retina in the far periphery, mid periphery and central region.

(a) Analysis with a linear mixed model indicates that the immunoreactivity levels of total tau, p-tau Ser202/Thr205, Thr217, Thr212/Ser214, Thr181 and Ser396 is significantly increased in the far peripheral region compared with mid periphery and central region (n=62). As the far peripheral region is used as a reference variable, it is not shown in the table. (**b)** Boxplots show the distribution of the average values of all cases (n=62) for total tau, p-tau Ser202/Thr205, Thr217, Thr212/Ser214, Thr181 and Ser396. Statistical analysis was performed using linear mixed model; *P value < 0.001.